UC San Diego
UC San Diego Previously Published Works

Title

Harmonizing DTI measurements across scanners to examine the development of white matter microstructure in 803 adolescents of the NCANDA study

Permalink

https://escholarship.org/uc/item/3qk056pt

Authors

Pohl, Kilian M

Sullivan, Edith V

Rohlfing, Torsten

et al.

Publication Date

2016-04-01

DOI

10.1016/j.neuroimage.2016.01.061

Peer reviewed

Harmonizing DTI Measurements across Scanners to Examine the Development of White Matter Microstructure in 803 Adolescents of the NCANDA Study

Kilian M. Pohl[1,2], **Edith V. Sullivan**[2,*], **Torsten Rohlfing**[1,†], **Weiwei Chu**[1], **Dongjin Kwon**[1,2], **B. Nolan Nichols**[1,2], **Yong Zhang**[2], **Sandra A. Brown**[3], **Susan F. Tapert**[3,4], **Kevin Cummins**[3], **Wesley K. Thompson**[3], **Ty Brumback**[3], **Ian M. Colrain**[1], **Fiona C. Baker**[1], **Devin Prouty**[1], **Michael D. De Bellis**[5], **James T. Voyvodic**[6], **Duncan B. Clark**[7], **Claudiu Schirda**[7], **Bonnie J. Nagel**[8], and **Adolf Pfefferbaum**[1,2]

1

2

3

4

5

6

7

8

Abstract

Neurodevelopment continues through adolescence, with notable maturation of white matter tracts comprising regional fiber systems progressing at different rates. To identify factors that could contribute to regional differences in white matter microstructure development, large samples of youth spanning adolescence to young adulthood are essential to parse these factors. Recruitment of adequate samples generally relies on multi-site consortia but comes with the challenge of merging data acquired on different platforms. In the current study, diffusion tensor imaging (DTI) data were acquired on GE and Siemens systems through the National Consortium on Alcohol and NeuroDevelopment in Adolescence (NCANDA), a multi-site study designed to track the trajectories of regional brain development during a time of high risk for initiating alcohol consumption. This cross-sectional analysis reports baseline Tract-Based Spatial Statistic (TBSS) of regional fractional anisotropy (FA), mean diffusivity (MD), axial diffusivity (L1), and radial

*Correspondence Edith V. Sullivan, Ph.D., Department of Psychiatry and Behavioral Sciences, Stanford University School of Medicine (MC5723), 401 Quarry Road, Stanford, CA 94305-5723, phone: (650) 859-2880, FAX: (650) 859-2743, edie@stanford.edu.
†Dr. Rohlfing's current affiliation is Google, Inc.

Author Manuscript

Author Manuscript

Author Manuscript

Author Manuscript

diffusivity (LT) from the five consortium sites on 671 adolescents who met no/low alcohol or drug consumption criteria and 132 adolescents with a history of exceeding consumption criteria. Harmonization of DTI metrics across manufacturers entailed the use of human-phantom data, acquired multiple times on each of three non-NCANDA participants at each site's MR system, to determine a manufacturer-specific correction factor. Application of the correction factor derived from human phantom data measured on MR systems from different manufacturers reduced the standard deviation of the DTI metrics for FA by almost a half, enabling harmonization of data that would have otherwise carried systematic error. Permutation testing supported the hypothesis of higher FA and lower diffusivity measures in older adolescents and indicated that, overall, the FA, MD, and L1 of the boys was higher than that of the girls, suggesting continued microstructural development notable in the boys. The contribution of demographic and clinical differences to DTI metrics was assessed with General Additive Models (GAM) testing for age, sex, and ethnicity differences in regional skeleton mean values. The results supported the primary study hypothesis that FA skeleton mean values in the no/low-drinking group were highest at different ages. When differences in intracranial volume were covaried, FA skeleton mean reached a maximum at younger ages in girls than boys and varied in magnitude with ethnicity. Our results, however, did not support the hypothesis that youth who exceeded exposure criteria would have lower FA or higher diffusivity measures than the no/low-drinking group; detecting the effects of excessive alcohol consumption during adolescence on DTI metrics may require longitudinal study.

Keywords

cortex; development; ethnicity; sex; adolescence; diffusion tensor imaging; fractional anisotropy

Introduction

White matter continues to grow in volume and mature in microstructural constituents from birth to late adolescence and early adulthood, as evidenced by convergent *in vivo* neuroimaging (Giedd et al., 1996; Im et al., 2008; Jernigan et al., 1991; Pfefferbaum et al., 1994; Sowell et al., 2004; Hasan et al., 2010; Lebel et al., 2008; Yeatman et al., 2014; Bava et al., 2010b) and postmortem (Benes et al., 1994; Yakovlev and Lecours, 1967) anatomical studies. The expansion of white matter, measured with structural MRI as increasing volume, and extension of tracts and myelin, measured as increasing fractional anisotropy (FA), decreasing axial diffusivity (L1), decreasing radial diffusivity (LT), or decreasing mean diffusivity (MD) with diffusion tensor imaging (DTI) (Barnea-Goraly et al., 2005; Lebel et al., 2008; Snook et al., 2005), complement the decline in developmental trajectories of cortical gray matter volume (e.g., Pfefferbaum et al., 2013; Raz et al., 2010) and thickness (Chen et al., 2013; Hogstrom et al., 2013; McKay et al., 2014; Schmitt et al., 2014; Sowell et al., 2007; Storsve et al., 2014). Consistent with these inverse relations, a multi-modal, cross-sectional imaging study of 932 youth, age 8 to 21 years, reported a correlation between lower mean diffusivity in white matter subjacent to regions of cortical thinning (Vandekar et al., 2015). Similarly, an inverse relation was observed between local FA and gray matter density in 42 adolescents (Giorgio et al., 2008) and cortical thickness in 168, 8 to 30 year olds (Tamnes et al., 2010a). These complementary dynamic growth patterns are presumed to reflect gray matter pruning of "unused" neurons (Chugani et al., 1987; Feinberg, 1974;

Feinberg, 1990; Feinberg et al., 1990; Huttenlocher, 1979; Huttenlocher and Dabholkar, 1997) and newly forming, extended, and increasingly complex fiber connections (Lenroot et al., 2007; Sowell et al., 2004), likely in response to interaction with the environment.

Adding to the complexity of neurodevelopment is heterochronicity in regional timing of maturation that characterizes gray matter volume decline and white matter volume increase (Bava et al., 2010b; Raznahan et al., 2012; Raznahan et al., 2010) (for review, Giedd et al., 2014; Stiles and Jernigan, 2010; Toga et al., 2006). The DTI metrics are especially useful in characterizing the major constituents of white matter, tracking changes through developmental periods, and identifying the maximum or minimum of diffusion MR-based measurements regressed with respect to age (Beaulieu, 2002). In particular, FA, a measure of local fiber organization, increases with age, from birth (Sadeghi et al., 2013) through late adolescence (Lebel et al., 2008) and beyond (Lebel et al., 2012; Tamnes et al., 2010a; Yeatman et al., 2014). Some studies report FA of the corpus callosum to be generally highest in early adolescence (Lebel et al., 2008), whereas others report later-occurring maxima in callosal FA (Asato et al., 2010; Hasan et al., 2009) and a posterior-to-anterior gradient of development (Asato et al., 2010; Cancelliere et al., 2013; Qiu et al., 2008). A fiber system showing continued development in adolescence is the superior longitudinal fasciculus (Peters et al., 2012). In summary, growth patterns estimated from cross-sectional study of children to older adults depict FA as increasing to late adolescence or early adulthood, with growth maxima differing by region (Hasan et al., 2010; Lebel et al., 2012; Yeatman et al., 2014).

The age and region of highest FA and lowest diffusivity vary substantially across reports and are likely attributable to many study differences, including scanner magnet field strength and manufacturer (Papinutto et al., 2013), acquisition protocol (Basser and Pierpaoli, 1996; Jones, 2004), quantification method, and participant factors such as age range (Yeatman et al., 2014), sex (Bava et al., 2011; Hasan et al., 2010; Herting et al., 2012; Wang et al., 2012), ethnicity, head motion (Kreilkamp et al., 2015; Yendiki et al., 2013), and even exercise (Herting et al., 2014). One way to confirm characterization of multifaceted dynamics of neurodevelopment is through longitudinal DTI study of adolescent white matter development. The few longitudinal studies currently published are consistent with cross-sectional observations in showing increasing FA throughout adolescence (Bava et al., 2010a; Giorgio et al., 2010; Treit et al., 2013; Wang et al., 2012) (review Paus, 2010). For example, one study examined 25 boys and girls, age 5 to 11 at baseline with about 2 to 4 years between scans, and observed continued FA increase in the callosal genu in the superior and inferior fronto-occipital fasciculi, superior longitudinal fasciculus, and uncinate fasciculus (Treit et al., 2013). Sex differences were detected in FA trajectories of 16 youth, age 13 to 17 years old, examined twice over one year, where boys showed continued increases in FA, whereas girls' trajectories were flat (Wang et al., 2012). The developmental increase in FA and axonal caliber has been linked to increase in testosterone with advancing puberty in boys (Herting et al., 2012; Perrin et al., 2008) but a decrease in FA with increasing estradiol in girls (Herting et al., 2012).

To date, longitudinal studies have been limited in scale with respect to sample size, subject factors, geographical representation, and age distribution. Large-scale, multi-site, cross-

sectional studies are an alternative to reconcile published cross-sectional findings on the growth patterns of microstructural white matter as they can provide critical steps to enhance consistency in across-site data collection (cf., Bartsch et al., 2014; Groves et al., 2012). To harmonize findings across sites, the Pharmacog Consortium developed a multi-site brain diffusion imaging protocol for 10 clinical 3T MRI sites distributed across four countries, whose reproducibility was comparable to those reported in studies using a smaller number of MRI scanners (Jovicich et al., 2014). Several studies (Bartsch et al., 2014; Kochunov et al., 2015) also proposed to normalize the measurements extracted from the diffusion MRI across sites. Specifically, the intensity values of a single gradient direction of a diffusion MRI are *relative* scores, whose meaning are defined in relation to the intensity values across all gradient directions. Normalizing the MR values directly requires solving a highly complex and non-linear mathematically framework that models the relation between those gradient directions. Instead, those studies proposed to normalize scores extracted across the diffusion directions contributing to diffusion metrics. For example, the ENIGMA-DTI consortium harmonized FA-based and genetics measurements collected from multiple sites by combining single-site heritability estimators with a multi-site correction model (Kochunov et al., 2015). Applied to five datasets containing a total of 2248 children and adults (ages 9 to 85 years), the model showed that genetic factors explained over 50% of intersubject variance in FA values across most regions (Kochunov et al., 2014).

Here, we proposed a 2-step approach to harmonize FA, MD, L1, and LT maps of multi-center DTI data by first accounting for differences potentially attributable to MR system manufacturer and then participant demographics and clinical scores. We harmonized DTI data acquired on scanners of two different manufacturers based on human-phantom data, i.e., repeated scanning of three non-participants on GE and Siemens scanners. Specifically, we inferred a scanner-specific correction factor from the human-phantom data and applied this correction factor to the DTI-derived maps of the study participants. The second step of data harmonization was based on statistical modeling with covariates defined by demographic and clinical markers. Specifically, skeletons were inferred from the manufacturer-corrected FA maps through Tract Based Spatial Statistics (TBSS) (Smith et al., 2006), which enabled a quantitative survey of white matter of the entire brain. A General Additive Model (GAM) with age, sex, self-described ethnicity, supratentorial volume, socioeconomic status, and pubertal development as covariates was applied to the regional FA, MD, L1, and LT skeleton mean values, which were computed by overlaying the skeletons onto the Johns Hopkins University (JHU) DTI atlas (Mori et al., 2005). In parallel, permutation testing was applied to the DTI metrics derived skeletons using sex and demeaned age as covariates.

Based on this 2-step approach, we present baseline findings on DTI data acquired in 803 adolescents (12-21 years old) through the multi-site National Consortium on Alcohol and NeuroDevelopment in Adolescence (NCANDA). The study is designed to follow adolescents annually for four years, an age range of significant neurodevelopment and high risk for initiating drinking, often at hazardous levels (MacArthur et al., 2012; Swendsen et al., 2012). The sample of 803 adolescents comprises two groups with useable DTI data: 671 adolescents who fell within established criteria for no to low alcohol and drug consumption

history, and 132 recruits who exceeded alcohol or drug consumption history at baseline. An extensive description of the total NCANDA sample (Brown et al., 2015), structural MRI baseline findings (Pfefferbaum et al., 2015b), and neuropsychological results (Sullivan et al., 2016) appear elsewhere.

Using these cross-sectional DTI measurements, we tested three hypotheses: 1) Corrected DTI metrics in the no/low-drinking group would reach extreme values at different ages in different fiber systems; specifically, FA would be highest at an earlier age in inferior and posterior fiber systems but at later ages in superior and anterior fiber systems. 2) Given that girls typically undergo pubertal development earlier than boys and that brain maturation has been shown to parallel pubertal stages, the highest FA and lowest diffusivity metrics would be at younger ages in girls than boys in the no/low-drinking group (cf., Herting et al., 2012; Hill et al., 2013; Perrin et al., 2008). 3) Although adults with a history of alcohol dependence and heavy or binge drinking are reported to have abnormally low FA and high diffusivity measures, the effects on white matter microstructure in youth with heavy alcohol exposure are less clear (for review, Elofson et al., 2013). Finally, we tested the hypothesis that youth who exceeded criteria for alcohol or other substance dependence would have lower FA or high diffusivity measures in later-developing fiber systems than the no/low-drinking group.

Methods

Herein are presented brief descriptions of the subject samples, the MR acquisition, the generation of the DTI-derived skeleton values harmonized for scanner difference, and the statistical models used for further harmonization of the data and analysis. A full description of the NCANDA recruitment strategies, sample, and demographics appear elsewhere (Brown et al., 2015).

Participants

The primary set of analyses focused on MRI data acquired across the five NCANDA recruitment sites (University of California San Diego, SRI International, Duke University Medical Center, University of Pittsburgh, and Oregon Health & Science University). Participants were 333 male and 338 female adolescents, ages 12 to 21 years (Table 1 and Figure 1, top) who met basic alcohol and drug use criteria (Figure 2) for history of no/low consumption in the NCANDA study (Brown et al., 2015). An additional 132 adolescents exceeded entry criteria for alcohol and drug use, having initiated moderate-to-high alcohol consumption (exceeds-criteria group); 9 of this group met criteria for DSM-IV Alcohol Abuse, and 1 met criteria for DSM-IV Alcohol Dependence. Using DSM5 criteria, 36 adolescents in the exceeds-criteria group endorsed having had alcohol symptoms; 19 met criteria for DSM5 Alcohol Use Symptoms in 12 month, and 13 meet criteria for DSM5 mild Alcohol Use Disorder Diagnosis. Thus, most participants in the exceeds-criteria group did not have a diagnosis of alcohol or substance use. The total group of 803 youth had useable DTI data and passed screening for anatomical anomalies determined by a clinical neuroradiologist (for clinical summaries, Pfefferbaum et al., 2015b).

Participants were characterized by age, sex, pubertal stage using the self-assessment Pubertal Development Scale (PDS) (Brown et al., 2012), socioeconomic status (SES) determined as the highest education achieved by either parent (Akshoomoff et al., 2014), and self-identified ethnicity (Table 1). Most subjects reported a single ethnicity (Caucasian, African-American, Asian, Pacific Islander, or Native American) with some reporting dual heritage. There were adequate numbers of the first three types to assign categorical ethnicity with dual-heritage identifications assigned to the minority ethnicity group (e.g., Asian-Caucasian was categorized as Asian) (Figure 1, bottom).

MRI acquisition

T1-weighted, 3D images were collected on the 803 adolescents in the sagittal plane on systems from two manufacturers: 3T General Electric (GE) Discovery MR750 at three sites (209 from UCSD; 157 from SRI; 171 from Duke) and 3T Siemens TIM TRIO scanners at two sites (118 from University of Pittsburgh; 148 from Oregon Health & Sciences University). The GE sites used an Array Spatial Sensitivity Encoding Technique (ASSET) for parallel and accelerated imaging with an 8-channel head coil and acquired an Inversion Recovery-SPoiled Gradient Recalled (IR-SPGR) echo sequence (TR=5.904ms, TI=400ms, TE=1.932ms, flip angle=11°, NEX=1, matrix=256×256, FOV=24cm, slice dimensions=1.2 × 0.9375 × 0.9375mm, 146 slices, ASSET=1, Acquisition Time=7m 16sec) and a 3D Sagittal CUBE T2 sequence (TR=2500, TE=80ms, ETL=100, matrix=256×256, FOV=24cm, slice dimensions=1.2 × 0.9375 × 0.9375mm, matrix=256×256, FOV=24cm, slice dimensions=1.2 × 0.9375 × 0.9375mm, 146 slices, Fat Sat=on, ASSET=4, Acquisition Time=3m 26sec). The Siemens sites used a 12-channel head coil to acquire a MPRAGE sequence (TR=1900ms, TI=900ms, TE=2.92 ms, flip angle=9°, NEX=1, matrix=256×256, FOV=24cm, slice dimensions=1.2 × 0.9375 × 0.9375mm, 160 slices, Acquisition Time=8m 8sec) and a T2 fast spin-echo (FSE) sequence (TR=3200ms, TE=404ms, matrix=256×256, FOV=24cm, slice dimensions=1.2 × 0.9375 × 0.9375mm, 160 slices, GRAPPA, Acceleration=2, Acquisition Time=4m 18sec).

To acquire Diffusion-Weighted Images (DWI), GE sites applied a 2D Axial Spin Echo, Echo-Planar protocol with two b=0/1000 and 60 directions (Acquisition Time: 8m 24sec) as well as a reverse-phase acquisition of the 2D Axial Spin Echo-Planar protocol (Acquisition Time: 1m 12sec) with b=0/500 and 6 directions (TR=10,000mm, TE=85mm, Thick=2.5mm, Number of Slices=64, FOV=24cm, xy_matrix=96×96, Phase = A/P, Partial k-space (48/64), Acceleration=2, Resolution=2.5×2.5×2.5mm, Fat Sat=on). The Siemens sites applied a 2D Axial Spin Echo, Echo-Planar protocol with two b=0/1000 and 60 directions (Acquisition Time: 8m 42sec), and a reverse-phase acquisition (Acquisition Time: 1m 22sec) with b=0/500 and 6 directions (TR=8,000ms, TE=89ms, Thick=2.5mm, Number of Slices=64, FOV=24cm, xy_matrix=96×96, GRAPPA, Acceleration=2, Resolution=2.5×2.5×2.5mm). The average of the two forward B0 acquisitions and the reverse acquisition were used for field inhomogeneity spatial distortion correction for both scanner systems.

Scalable Informatics for Biomedical Imaging Studies (SIBIS)

The data of this manuscript were based on a formal, locked data release (VERSION: NCANDA_DATA_00012) provided by the software platform Scalable Informatics for

Biomedical Imaging Studies (SIBIS; https://github.com/sibis-platform). SIBIS consists of IT infrastructure for collecting behavioral and imaging data at the NCANDA sites, Internet, and application programming interfaces for uploading the acquired data to a central biomedical data repository, a validated workflow to perform quality control, a multi-modal image processing pipeline for computing FA maps, a phantom-based normalization of Tract-Based Spatial Statistics (TBSS) across manufactures, and a release mechanism for disseminating the data to be used for publications. We now briefly review the individual components of this platform. Additional information about the non-imaging component of SIBIS has been published elsewhere (Nichols and Pohl, 2015; Rohlfing et al., 2014).

Infrastructure for data collection and uploading—The infrastructure for collecting data included the Research Electronic Data Capture (REDCap; http://project-redcap.org) system (Harris et al., 2009), LimeSurvey (http://www.limesurvey.org), Blaise (http://www.blaise.com), and eXtensible Neuroimaging Archive Toolkit (XNAT; http://www.xnat.org). Data collected via computer were automatically merged onto a REDCap server hosted at the NCANDA Data Analysis Component at SRI International. Imaging data were first uploaded from the site-specific Picture Archiving and Communication Systems (PACS) to an XNAT server hosted at SRI International.

Quality control—Once archived in XNAT, the quality of the images was checked, which included evaluation by a clinical neuroradiologist and review of automatically generated image scores described in further detail as part of the Image Processing section. Finally, the outcome of the quality control was uploaded into REDCap and merged with the corresponding non-imaging data for each session. Any updates to information in the REDCap database automatically triggered SIBIS to generate reports regarding data integrity. The data manager (W.C.) checked these reports on a biweekly basis and consulted with site testers to resolve data entry or scoring irregularities.

Image processing—SIBIS first processed the structural images and then used the results to generate summary scores of the DWI sequences. Specifically, the T1- and T2-weighted images were bias field corrected and the T2-weighted images were rigidly aligned to the corresponding T1-weighted scans via Computational Morphometry Toolkit (CMTK) (https://www.nitrc.org/projects/cmtk/). The T1-weighted images were skull stripped, which was the result of majority voting (Rohlfing et al., 2004) applied to the maps extracted by the Robust Brain Extraction (ROBEX) method (Iglesias et al., 2011) and FSL Brain Extraction Tool (Smith, 2002) run on both T1- and T2-weighted scans. Finally, baseline skull-stripped T1-weighted images were registered to the T1-weighted channel of the SRI24 atlas (http://nitrc.org/projects/sri24) (Rohlfing et al., 2010), the standard space for group-vise analysis of SIBIS, via nonrigid image registration (http://nitrc.org/projects/cmtk) (Rohlfing et al., 2003a; Rohlfing et al., 2003b).

As part of quality control, the pipeline excluded bad single shots, which were defined by the root mean square power deviation, based on all 60 directions for a given slice. Echo-planar structural distortion was corrected using the b=0 reverse and forward readout data, i.e., the "pepolar" procedure (Holland et al., 2010), also implemented in CMTK. Eddy-current-induced image distortions for each direction were then minimized by first aligning each of

the 60 directions of the pepolar-corrected data to the pepolar-corrected B0 image using a 2D, 6-parameter affine correction (translation and shear) on a slice-by-slice basis. Each distortion-corrected direction was rigidly aligned to the average across all 60 directions to correct for motion. For quality control, the pipeline recorded the average magnitude of the translational components and the average absolute value of the rotational components of all rigid transformations. Omitted from further analysis were those directions whose combined rotational motion across the three axes was larger than 3 degrees. The remainder of the pipeline confined analysis to the forward acquisition corrected with respect to distortion and motion.

To compute FA, MD, L1, and LT maps from the DWI, we first skull-stripped the images by non-rigidly aligning the T1-weighted image to the B0 image of the corrected forward acquisition (http://nitrc.org/projects/cmtk) (Rohlfing et al., 2003a; Rohlfing et al., 2003b) and applying the resulting deformation field to the brain mask of the T1-weighted image. At this point, the pipeline checked again the quality of the data by searching for clear outliers in regional intensity ranges of the skull stripped DWI images and the signal-to-noise ratio (SNR) of the corresponding B0 scans with respect to the corpus callosum. We then computed the diffusion tensor image from the DWI by applying CAMINO's linear single tensor model approach (Cook et al., 2006) and inferred from the resulting Diffusion Tensor images the FA, MD, L1, and LT maps.

To achieve common anatomical coordinates across subjects, each subject's DWI derived data set was registered to the FA channel of the SRI24 atlas (Rohlfing et al., 2010). Alignment of subject FA to SRI24 atlas space was initialized by concatenating the previously computed atlas-to-subject T1-weighted transformation with the subject T1-to-subject DTI transformation. To this concatenation was fit a single, coarse B-spline nonrigid transformation, which was then refined using intensity-driven registration of the SRI24 atlas FA to subject FA image. The resulting non-rigid transformation was then also applied to MD, L1, and LT maps to align them with the SRI24 atlas.

Phantom-based normalization of Tract-Based Spatial Statistics (TBSS)—To compute the TBBS skeletons (Smith et al., 2006), we first corrected the DWI derived maps for scanner-specific differences across the sites. Accordingly, we acquired 26 DWI scans (University of California San Diego: 5 visits; SRI International: 6 visits; Duke University Medical Center: 6 visits; University of Pittsburgh: 3 visits; Oregon Health & Science University: 6 visits) from three human phantoms, not part of the study participant group, that travelled to all five sites, two or more times each. Specifically, two women (age 30 and 64) and one man (age 41) visited at least one and no more than two times each site. The average time between baseline and follow up visit for each site was 357 days with a standard deviation of 37 days. We then computed the mean FA, MD, L1, and LT values of each scan with respect to the full-atlas parcellation defined by the JHU DTI Atlas (Mori et al., 2005). To do so, the FA image of the JHU atlases in FSL was registered to the FA channel of the SRI24 atlas, both at $1mm^3$ pixel size, using a linear, affine registration, based on the normalized cross-correlation similarity measure. Next, the two FA images were nonrigidly registered based on a coarse B-spline grid, which avoids overfitting. Labels from the JHU-ICBM atlas were then mapped into SRI24 space via reslicing of the JHU label map using the

nonrigid transformation and partial volume interpolation. Left and right unilateral atlas locations were combined, resulting in 21 bilateral and 6 midline regions from which the mask was inferred. For each scan, we computed the mean FA, MD, L1, and LT values of this mask (Figure 3). With the exception of L1, Figure 3 shows for each subject two clusters (red and blue) clearly separated according to the associated manufacturer type. We therefore corrected each map of the NCANDA sample associated with the Siemens scan by applying the ratio between the two scanner types with respect to the mean values across the 26 human phantom visits: Mean FA GE / Mean FA Siemens = 0.916; Mean MD GE / Mean MD Siemens = 1.035; Mean L1 GE / Mean L1 Siemens = 0.996; Mean LT GE / Mean LT Siemens = 1.077). Figure 3 shows the corrected Siemens scores of the human phantoms in green, whose clusters after correction now better align with the GE ones, especially for FA, LT, and MD. To estimate the error associated with these correction factors, we recomputed the correction factor for each phantom visit at a Siemens scan paired with all its visits at GE sites. Based on the resulted 51 factors per modality, the mean and standard deviation for FA = 0.901 ± 0.029; for MD = 1.046 ± 0.024; for L1 = 0.999 ± 0.015; and for LT = 1.096 ± 0.037. Computing the correction ratio based on the maps of all 803 subjects resulted in a similar outcomes to the ratios based on the three human phantoms: Mean FA GE / Mean FA Siemens = 0.916; Mean MD GE / Mean MD Siemens = 1.040; Mean L1 GE / Mean L1 Siemens = 0.999; and Mean LT GE / Mean LT Siemens = 1.085. All of these scores were within one standard deviation of the human phantom based ratios so that the difference in age between the human phantoms and the NCANDA samples was statistically insignificant for these computations. Notably, using the ratio based on the non-NCANDA phantom data rather than on NCANDA samples avoided using the dependent measures to correct themselves. Furthermore, the error between scanner types substantially dropped from before to after correction for FA, MD, and LT. We inferred the error by pairing each phantom visit at a Siemens scan with the closest visit within 30 days of the same phantom at a GE site (average number of days between visits was 14.9 days) and then computed the absolute difference between the paired mean values. The average error between the resulting 7 paired FA mean values without correction was 0.04668, which was almost 6 times higher than the error after applying the ratio to the Siemens scans (average error: 0.0078). For the other modalities the error dropped from 0.000032 to 0.000015 for MD, from 0.000019 to 0.000018 for L1, and from 0.000106 to 0.000028 for LT.

Finally, the FA-corrected maps of the 803 subjects were transformed into FA skeletons via TBSS, omitting the standard registration step of TBSS as the FA maps were already aligned to the SRI24 atlas. Applying the result template of a skeleton to the other modalities, we created the MD, L1, and LT skeletons according to TBSS protocol. For each modality, we reduced each skeleton to the skeleton mean values of 28 regions, which were defined according to the JHU atlas and its mask. The data presented in Results are mean values for the FA, MD, L1, and LT skeletons for the JHU regions of interest, but referred to simply as "FA, "MD," "L1," and "LT." Finally, we checked the quality of the data by investigating outliers in average regional scores, which all scans passed.

Data release—To create the data release for this publication, all entries in the NCANDA REDCap database and the previous image processing steps were manually checked for entry

errors. Entries passing quality control were locked in the database, i.e., changes to these records required prior approval by the NCANDA Data Analysis component investigators. With respect to incorrect or questionable entries, the data manager resolved the issues by contacting the collection sites and locked the record once the error was resolved. After all entries requested for the data release were locked, the platform created a data release by exporting comma-separated-value (CSV) files and corresponding data dictionaries for each data element from REDCap and archived the original and processed imaging files as well as then-current copies of all processing scripts and software tools on a dedicated file server. Finally, this archived set of files was then assigned a permanent name for reference and identification.

Statistical analysis of manufacturer-corrected FA skeletons

Based on the data release, the predictive value of the main effect of age was tested with selected covariates within the no/low drinkers using GAM (Hastie and Tibshirani, 1986, 1990; Wood, 2006, 2011) and permutation testing. A second set of analyses examined differences between the no/low alcohol-use and the exceeds-criteria groups.

To test the predictive value of the main effect of age with respect to the region-specific, manufacturer-corrected mean skeleton values, the GAM was complemented with analysis of variance (ANOVA) from the "mgcv" package in R Version 3.1.0 [http://www.r-project.org/] separately for each DTI metric. Values of each dependent brain measure were potentially modulated by sex, supratentorial volume (svol), ethnicity, pubertal development (measured with the Pubertal Development Scale (PDS, Brown et al., 2012)), and Socioeconomic Status (SES, estimated as highest parental education achieved (cf., Akshoomoff et al., 2014)). We chose supratentorial volume (svol) over intracranial volume (ICV) as a covariate in our model because although these volumes highly correlated (r=0.993), the inferior boundary of ICV is generally poor defined and includes pouches of CSF that can incorporate anomalous volumes, as occurs with mega cisterna magna (incidence of these anomalies was 22 (~3%) in the total sample of 803 participants (Pfefferbaum et al., 2015b).

The contributions of these covariates were examined in a step-wise manner with sub-models excluding various covariates and categorical predictions. The initial GAM tested the predictive value of age alone. Visual inspection of the data suggested a nonlinear function with maximum FA achieved prior to the oldest age. Therefore, differences in regional, manufacturer-corrected Skeleton Mean values (FA-SM, L1-SM, LT-SM, MD-SM) associated with age were modeled with a thin-plate spline (TPS).

Subsequent GAMs tested age with one or more covariates to enable assessment of the influence of each covariate on the distribution of the dependent measure for each ROI with the full GAM model with respect to region 'r' and subject 'i' being defined for (X=FA,L1,LT,MD) as

$$X-SM_{r,i} \sim \beta_0\left(r\right) +\beta_1\left(r\right)\cdot TPS\left(r, \mathrm{age}\right)+\beta_2\left(r\right)\cdot \mathrm{ethnicity}_i+\beta_3\left(r\right)\cdot \mathrm{sex}_i+\beta_4\left(r\right)\cdot svol_i+\beta_5\left(r\right)\cdot SES_i+\beta_5\left(r\right)\cdot PDS_i.$$

For each region, we fitted GAMs confined to a subset of covariates to the X-SM values of all subjects. The sample sizes varied slightly across models tested because not all participants had data for SES, PDS, or fell into the three major ethnicities. Restricting the analysis from the full model to covariates showing a significant effect on the FA-SM values (age, sex, ethnicity, and svol), we compared the outcome to the GAM model for FA without covariates and, inspired by PING (Bartsch et al., 2014), applied our proposed GAM with additional covariate being manufacturer to the original FA Skeleton Mean values (without correction). For each of the FA based GAM models, we computed the 99% confidence interval of the age associated with the maximum value of the age-associated thin plate spline function *TPS(r,·)* by bootstrapping (using 1000 iterations) the fitting of *TPS(r,·) to the* residuals of the models (excluding age). We interpreted the resulting age range as the highest degree of fiber organization of the no/low alcohol drinkers in the 12-21 age group. For the diffusivity metrics, we similarly investigated the 99% confidence interval of the minimum of their thin plate spline function *TPS(r,·).* In this analysis, the age associated with the highest degree of fiber organization is limited to the age range of the NCANDA study, i.e., 12 – 21 years, and thus makes no inference effects outside of that range. Finally, we use the GAM to investigate differences between the no/low and the exceeds-criteria groups.

In parallel with the GAM-based analysis, we investigated for each DTI metric differences between the groups on the manufacturer-harmonized skeleton scores via FSL's method for permutation testing, "TFCE Randomise" (Threshold-Free Cluster Enhancement). The testing was confined to 500 permutations, used no/low group vs. exceeds-criteria group as the contrast, and included the covariates sex and age, with the latter demeaned. Statistical inference was performed with the TBSS "corrp" option (fully corrected for multiple comparisons across space), hereinafter referred to as "tfce_corrp" (Smith et al., 2006). To confirm findings, the analysis was repeated on a subgroup of 101 adolescents in the no/low-drinking group and 116 with adolescents from the exceeds-criteria group. The two subgroups were matched with respect to age, sex, and ethnicity. Furthermore, we repeated the analysis on the no/low group using sex as contrast and demeaned age as covariate to investigate the effect of sex and age.

Results

Effect of manufacturer harmonization on the 671 no/low-drinking group

Figure 4 (left) shows the distribution of the mean of the uncorrected skeleton values (Global Mean FA, MD, L1, and LT) across the 671 no/low-drinking adolescents plotted against age. For each adolescent, the mean was computed from the uncorrected values inside the mask defined by the JHU atlas. Blue shows the mean value of samples scanned on 3T Siemens TIM TRIO scanners. For any age group, the mean FA values are generally higher and for MD and LT lower than those acquired on 3T General Electric Discovery MR750 scanners (brown circles), which is also reflected by the average SNR with respect to the corpus callosum of the Siemens data (SNR: 2.8514) being lower than those of the GE data (SNR: 3.1962). The dark gray lines in Figure 4 are the linear regression of all measurements across time and the dotted lines are the first and second standard deviations. Figure 4 (right) shows the corresponding plots of the means of the manufactured-corrected values. The

measurements regress to lines that are similar in slope to the ones regressed from the uncorrected scores. With the exception of L1, which were not related to manufacturer, the variance within these samples with respect to FA, MD, and LT became substantially smaller; the standard error of the regression (i.e., the standard deviation after removing the regression on age) of FA was reduced from 0.0246 to 0.0138, for MD from 0.0000265 to 0.0000230, for L1 from 0.0000261 to 0.0000260, and for LT from 0.0000628 to 0.0000491.

Table 2 presents the age associated with the maximum of the regressed spline function for the proposed GAM model applied to the manufacturer-correct FA skeleton mean values and the PING inspired GAM model applied to the original skeleton FA means. The difference between the maximum of the age-regressed curves computed by both models was within one year for 20 out of 28 regions and for 23 regions the difference was less than 2 years. For one region, our regression did not report a maximum but the PING inspired model did with corresponding ages in the late adolescence (age 19). For the remaining 4 regions, ages below 19 were associated with the maximum of our proposed regression model while the PING inspired model did not report a maximum within the age range.

Table 3 presents the age associated with the minimum of the regressed spline function for the proposed GAM model applied to the manufacturer-corrected MD, L1, and LT skeleton mean values. The effect of age on those measurements was less pronounced, with L1 only showing age differences in 3 regions, LT only 4 regions, and MD only 5 regions that peaked with 99% confidence within the age range of 12 to 21. These regions were also identified by our FA-based model with the exception of the corticospinal tract, for which both MD and LT identified the minimum of the regression model at age 16, and the pontine crossing fibers, for which L1 identified the minimum of the regression model at age 18. The age associated with 8 out of the remaining 9 regions was within one year of our FA regression model

Permutation testing applied to the no/low-drinking group (N=671)

To investigate the contributions of sex and age, permutation testing was limited to the skeletons of the 671 no/low-drinking participants (338 girls, 333 boys) using sex as a contrast and age as a covariate. Our analysis detected significantly higher skeleton values (p < 0.01), corrected for manufacturer, for boys (voxels with significant higher skeleton are shown in blue in Figure 5, left) for FA, MD, and LT. Furthermore, testing discovered higher FA and lower MD, L1, and LT along almost the entire skeleton with older age (Figure 5).

GAM applied to the no/low-drinking group (N=671)

The dependent measures were regional and global FA skeleton mean values of the 671 no/low-drinking adolescents and the primary independent measure was age. Depending on the factor examined, sex, supratentorial volume (svol), ethnicity (representing Caucasian, African-American, Asian, and Other), SES, or PDS were entered as model covariates. A conservative level of significance was determined as p .002, based on Bonferroni correction for 28 ROIs with α=.05.

Age—The initial GAM tested the predictive value on regional and whole brain FA of age alone without consideration of covariates. The percent deviance explained was significant for 25 of the 28 regions (Table 2), including the global measure, and ranged from 1.2% for the retro-internal capsule to 15.7% in the cerebral peduncles. The exceptions, that is, with no significant deviation explained, were the FA skeleton mean values of the pontine, pontine crossing fibers, the fornix, and uncinate. With respect to movement measured according to average absolute rotation and normed translation, Figure S1 (see Supplement) shows heteroscedasticity at younger ages, but the correlation with respect to age was not statistically significant.

Sex—Expanding the model to examine sex indicated lower FA in female than male adolescents in all but 5 regions (including the global measure), and this difference was significant (p .002) in 4 regions. Recognizing the substantial sex difference in svol (t=17.475, p=.0000), we included svol as a covariate. This analysis partly reversed the sex effects, such that the FA of the girls was significantly higher than that of the boys in 3 regions (pontine crossing, inferior cerebellar peduncle, and stria terminalis). Whereas girls had significantly higher L1 in the inferior cerebellar peduncle, pontine crossing fibers, and 2 other regions (external capsule and retrosplenial internal capsule), boys had higher L1 values in the splenium and higher LT values in the stria terminalis and in the pontine crossing fibers. MD showed no significant sex differences. The sex differences in the DTI derived measurements were not affected by motion as the difference in motion represented by the average absolute rotation and normed see also Figure S1, top).

Ethnicity—To examine the contribution of ethnicity to regional FA skeleton mean values, we included ethnicity together with sex and svol in the model because svol was found to be significantly smaller in our sample of non-Caucasian relative to Caucasian participants. Relative to the Caucasian adolescents, African-American adolescents had significantly higher FA in the global plus 9 regions (Figures 6-12) and significantly higher MD in 5 regions, lower L1 in 6 regions, and lower LT in 2 regions (Supplemental Figures S2-9). Asian adolescents had lower FA than Caucasian adolescents in 5 regions (inferior cerebellar peduncle, retro-internal capsule, posterior thalamic fibers, fornix, and sagittal stratum). Asian adolescent had higher MD in the posterior thalamic fibers, higher L1 in the tapetum, and higher LT in all fiber systems except the fornix. Motion values were not statically significantly different between African-American and Caucasians nor between Asians and Caucasian adolescents (Figure S1 bottom).

Pubertal Development Scale and Socioeconomic Status—Of the 671 individuals included in the primary analysis, 639 had both PDS and SES scores. Neither PDS nor SES significantly contributed to the model for any region examined; thus, neither factor was used in further analyses.

Modeling differences over the adolescent age range—A GAM that included sex, ethnicity, and svol as covariates to model age yielded significant (p .002) age effects in 21 of the 28 regions, where higher FA occurred in older adolescents, and explained 3.9% to 17.0% of the deviance. Significant age effects with lower values occurring in older

adolescents were detected by MD in 24 regions, by L1 in 14 regions, and by LT in 25 regions and explained 3.1% to 22.2% of the deviance. F-tests identified that the spline curve modeled age better than a linear fit in 25 of the 28 regions for FA (Table 2 and Figures 6-12), 26 regions for MD, 14 regions for the L1, and 24 regions for the LT (Table 3 and Figures S2-9). The 99% confidence interval for the highest FA over age was estimated by repeatedly computing the maximum value of the spline function via Bootstrapping. The region at which FA skeleton mean values where the highest at the youngest age was the corpus callosum, specifically, the genu. FA did not regress to a maximum within the age range 12 to 21 years in 12 regions, 11 of which were confirmed by the PING-inspired model and the other DTI metrics, and appeared to have the potential for further increase at ages beyond those tested in this sample (Table 2 and 3; and Figure S2 – S9).

Comparison of no/low vs. exceeds-criteria groups: GAM and permutation testing

The manufacturer-corrected FA skeleton mean values of the 671 no/low-drinking participants were compared with the 132 adolescents in the exceeds-criteria group using the GAM, covarying for ethnicity, sex, and svol. In no case did the exceeds-criteria group have lower FA than the no/low group. Rather, FA was higher in the exceeds-criteria than the no/low-drinkers in 5 regions: middle and superior cerebellar peduncle, callosal body, medial lemniscus, and posterior internal capsule.

Among the 132 adolescents in the exceeds-criteria group, 112 reported one or more binges in the past year, ranging from 1 to 137 episodes. A GAM, testing the predictive value of age, ethnicity, and sex plus the number of binges in the past year, was conducted for each brain metric among the 132 exceeds participants. In no fiber system was the FA skeleton mean value significantly related to the number of binges in the previous year.

We applied FSL's "TFCE Randomise" technique to the skeletons of the manufacturer-corrected FA values of a data set where 101 no/low-exposure participants had been matched to 116 adolescents from the exceeds-criteria group with respect to age, sex, and ethnicity. Covariates of the permutation model were demeaned age and sex. The comparison resulted in no significant group differences ($p < 0.01$). This was also the case when the analysis was repeated on the entire, unmatched data set (the skeletons of 671 no/low-drinking vs. 132 exceeds-criteria adolescents) and for the diffusivity metrics.

Discussion

To reduce variation within the DTI-based measurements unrelated to factors exclusive of the primary study hypotheses, we applied a 2-step harmonization approach to the multi-site NCANDA data. Harmonizing FA, MD, L1, and LT maps across manufacturers entailed the use of human-phantom data to determine a scanner-specific correction factor. In addition, statistical analyses accounted for potential demographic and clinical effected by covariation in the statistical models. Specifically, GAMs tested for age and sex differences in mean FA, MD, L1, and LT skeletons in regions defined by the JHU DTI atlas (Mori et al., 2005).

The results supported the primary study hypothesis that FA in the no/low-drinking group reached maximum values at different ages, and when differences in supratentorial volume

were covaried, FA skeleton mean reached their highest values at younger ages in girls than boys in the no/low-drinking group. The PING inspired GAM model comported with those findings. Furthermore, permutation testing supported the hypothesis of higher FA in older adolescents and indicated that, in general and irrespective of age, the FA of the boys was higher than that in the girls, suggestive of continued microstructural development notable in the boys. The permutation testing of the diffusivity metrics complemented FA findings, where diffusivity was lower in older adolescents and L1 and MD was generally higher in boys than girls. By contrast, our results did not support the hypothesis that youth who exceeded exposure criteria would have lower FA or higher diffusivity than the no/low-drinking group; instead, the exceeds group had modestly higher FA than the no/low-drinking group, in several fiber systems. These findings are discussed next.

Data harmonization across MR system manufacturers

The systematic difference in FA, MD, and LT values produced by the two MR system manufacturers of the NCANDA study precluded combining DTI data without devising an adequate correction factor given that FA from the Siemens scanners was significantly higher than FA from the GE scanners and LT and MD from the Siemens scanners was significantly lower than the corresponding measures from the GE scanners. This difference occurred despite installation of equivalent image acquisition parameters between platforms and use of two acquisitions with opposite diffusion gradient polarity ("pepolar") (Bodammer et al., 2004; Holland et al., 2010) to minimize spatial distortion induced by B0 susceptibility as the average SNR of the GE scans (SNR: 3.1962) was substantially higher than that of the Siemens scans (SNR: 2.8514). Further, given the known effects of spectral spatial pulses versus fat saturation on slice profile and, therefore, voxel volume, we chose to use fat suppression on both scanner systems, eliminating slice profile as one explanation of scanner differences (Glover et al., 2012; Liu et al., 2010). Traditionally, acquisition differences due to site differences have been incorporated as a covariate in the statistical model, such as in the PING inspired GAM and other published models (Bartsch et al., 2014; White et al., 2011), thus decreasing the model's degree of freedom. Instead, we introduced a correction factor determined from measurements acquired from human phantoms whose standard deviation for the FA-based correction factors bracketed the one based on the ratio between the SNRs of the scanner types (SNR of Siemens / SNR of GE = 0.892). Lower SNR can lead to higher FA and lower MD and LT estimates, especially for TBBS, which searches for the highest FA values in a region.

Imaging phantom data, such as from the ADNI phantom [http://www.phantomlab.com/products/magphan_adni.php], are also acquired by the NCANDA sites along with structural MRIs of humans to capture spatial distortion and variability across time and scanner platforms for harmonization of structural data. Beyond spatial distortion, designing imaging phantoms to capture fully and accurately the variation in diffusion-weighted, human brain measures across manufacturers remains an open challenge in biomedical engineering. One can, however, use human phantoms, such as in the NCANDA study, which acquired MR imaging data on the same three non-NCANDA participants repeatedly at all five collection sites. For this analysis, we used these data to determine a manufacturer-specific correction factor for FA, MD, L1, and LT values. The resulting corrected data produced age-regression

slopes that were similar to the slopes produced with the uncorrected data, indicating that the adjustment did not introduce an emergent effect. Critically, the distributions of corrected scores from the two different scanner manufacturers were essentially overlapping. Furthermore, the standard error of the regression was reduced by almost a half for FA, by 13% for MD, by 22% for LT, but had only had a minor effect on L1. Thus, the human phantom data proved crucial for harmonizing the FA, LT and MD measurements derived from this multi-site DTI set.

Heterochronicity in the ages associated with maximum FA skeleton means of major fiber systems

Globally and regionally, the FA age regressions of JHU atlas-defined fiber tracts (Hua et al., 2009) were generally better fit with a spline than a linear function, which was also the case for LT and MD based regressions. This approach enabled identification of the age at which the spline reached a maximum value within a 99% confidence interval. For FA, exceptions in identifying a peak value were the pontine crossing fibers, fornix, and uncinate fasciculus, suggesting continued development of FA in these fibers beyond the age range of the current sample, which ended at 21.9 years. These findings were also confirmed by the PING-inspired GAM model and less pronounced for the diffusivity metrics. The spline-fit age regression of the global FA skeleton revealed evidence for continued fiber organization in boys and girls up to 18 years.

Commissural fibers—Regionally, the age at which the regressed FA values reached their maximum varied by fiber system but seldom by sex. For commissural fibers of the genu, body, and splenium, the ages associated with the maxima were around the age of 17 years. The PING-inspired GAM model confirmed maxima for the genu and body but at a later age. For the tapetum, the spline of our GAM model did not have a maximum. Early development of commissural tracts (also reported by Lebel et al., 2012; Lebel et al., 2008; Schneiderman et al., 2007) is essential for robust interhemispheric communication and coordinated functions, including integration of semantics and prosody in speech and language (Fryer et al., 2008) and bilateral motor control (Barral et al., 2006; de Boer et al., 2012; Marion et al., 2003; Muetzel et al., 2008) as also required in sports, which advances during adolescence.

Brainstem projection fibers—Of the five brainstem projection fibers, only the middle cerebellar peduncle had a highest regressed FA mean value at an age (approximately 18 years) that was younger than the maximum studied (cf., Simmonds et al., 2014). This finding was supported by MD, whose lowest regressed mean value was also at that age. In the second set of projection fibers, 8 of the 10 corticospinal tracts had the highest FA skeleton mean values in the late teen years, 5 of which were confirmed by the PING-inspired GAM within one year. The two exceptions that had no maximum FA skeleton mean value were the principal corticospinal tract, serving postural stability, and the medial lemniscus, which also failed to identify minimum skeleton values for MD, L1, and LT, serving touch, vibratory, and pressure sensation through connections with the thalamus (Ross, 1991).

Association fibers—A common focus of developmental studies of brain microstructure is the system of association fibers because of their role in high-order, cognitive functions that require integration of far-reaching cortical systems (cf., Dick and Tremblay, 2012; Martino and De Lucas, 2014). All four of the limbic tracts were characterized by a continued rise of FA into young adulthood, which was also confirmed by the GAM. The fornix is a principal connector of limbic circuitry, including Papez circuit, underlying components of declarative memory. Similarly, the inferior cingulum, which makes up the temporal stem, is a conduit to medial temporal, hippocampal function, including memory consolidation (Squire and Zola-Morgan, 1991), in addition to communication with posterior parietal sites. Disruption of these limbic fiber systems in Alzheimer's disease (AD) contributes to the episodic memory (Nowrangi et al., 2013; Salat et al., 2010; Zhuang et al., 2013) and visuospatial dysfunction common in AD patients (Jacobs et al., 2015), characteristic of a disconnection-like syndrome (O'Sullivan et al., 2001; Sullivan, 2003). The anterior/middle cingulate bundle supports communication relevant to high-order, attentional processing, which continues to mature into young adulthood (for review, Stiles and Jernigan, 2010). The stria terminalis provides structural connectivity among the amygdala, septal nuclei, hypothalamus, and thalamus and intersects with the hypothalamic-pituitary-adrenal axis. These regions and systems are involved in pubertal development, stress modulation, threat monitoring, and addiction (e.g., Koob, 2009).

Association fasciculi—The superior longitudinal fasciculus and superior frontal-occipital fasciculus exhibited the highest regressed FA mean values around age 18, which was confirmed by the PING-inspired GAM, and around age 19 for the sagittal stratum, which the GAM moved to age 20. No model detected a maximum for the uncinate fasciculus, which is reported to develop with reading and language skills (Paldino et al., 2014). These late-developing fiber systems included the superior longitudinal fasciculus, which has been identified in meta-analyses as the tract most consistently reported to be associated with continued development (Peters et al., 2012) and integral to selective functions of verbal fluency, reading (Hoeft et al., 2011; Zhang et al., 2014), vocabulary (Tamnes et al., 2010b), and working memory (Ostby et al., 2011; Vestergaard et al., 2011). Other late-developing tracts were the superior frontal occipital fasciculus (for background, Schmahmann and Pandya, 2007), damage to which has been found in spatial neglect (Shinoura et al., 2009; Shinoura et al., 2010), and the sagittal stratum, which intersects with language areas (Menjot de Champfleur et al., 2013) and, along with other association fasciculi, can sustain microstructural damage with functional ramifications following traumatic brain injury (Farbota et al., 2014).

Factors modulating FA in adolescence

Sex—Few sex differences were forthcoming when age was controlled for as a factor. Observation of sex differences, where boy had higher FA than girls, depended on whether supratentorial volume was considered in the GAM. Exceptions were the stria terminalis, inferior cerebellar peduncle, and pontine crossing fibers, where FA was higher in female than male groups. The girls also had higher LT in the stria terminalis and higher L1 in the inferior cerebellar peduncle and pontine crossing fibers than the male group. The earlier maturity of girls compared with boys was evident in longitudinal study of mid-adolescents

that showed the regressed FA mean values to be highest at younger ages in girls than boys (Wang et al., 2012). A 4-year longitudinal study of healthy youth, 12-14 years old at initial DTI, found that in general girls showed earlier FA increases in motor-related tracts than boys, whereas boys showed greater changes in projection and association tracts, although these sex differences were not statistically related to pubertal status (Bava et al., 2011). A larger-scale, longitudinal DTI study also focused on white matter microstructural development in adolescence and observed that, whereas girls exhibited evidence for white matter maturation through mid-adolescence, boys' changes continued through early adulthood (Simmonds et al., 2014). As observed in the current study, later-developing fiber systems included corticolimbic tracts.

Ethnicity—Ethnicity also contributed to variance. The most consistent pattern was higher FA in African-Americans, who comprised 12.5% of the no/low-drinking group, than in Asians (7.7%) or Caucasians (70.3%). This pattern held for FA in the whole atlas and regionally in the middle cerebellar peduncle, anterior corona radiata, corticospinal tract, internal and external capsule, anterior middle cingulum, and superior frontal occipital fasciculus. In these regions, African-Americans had higher L1 in the anterior corona radiata and lower LT and MD in the middle cerebellar peduncle and internal capsule relative to Caucasians. In the splenium, Asians and African Americans had higher FA than Caucasians. These ethnic differences were identified with the GAM, which covaried for sex, supratentorial volume, and ethnicity, and, therefore, found ethnicity differences in excess of those accounted by the statistical model.

Alcohol use—Although in our structural MRI study of regional white matter volumes in the NCANDA cohort did not detect deficits in youth who exceeded criteria for drinking compared with the no/low-drinking youth (Pfefferbaum et al., 2015b), we pursued the hypothesis that regional FA deficits would be apparent in the exceed-criteria group for two salient reasons: 1) other studies identified FA deficits in heavy-drinking youth (Bava et al., 2013; Jacobus et al., 2009; Jacobus et al., 2013) (for review, Elofson et al., 2013) and 2) FA deficits have been found in adult alcoholics who did not have white matter volume deficits (Pfefferbaum et al., 2014; Pfefferbaum and Sullivan, 2002). Further, because our structural MRI study of NCANDA youth found that smaller central white matter volumes were modestly correlated with greater numbers of lifetime drinks, we proposed the hypotheses, which were not supported herein, that DTI metrics in the exceeds-criteria group would be related to amount drunk. A notable difference in the current study is that the amount of alcohol consumed was less intense and less frequent here. In addition, youth in previous studies were commonly recruited from treatment facilities and drank sufficiently to have a DSM diagnosis, whereas all NCANDA youth, despite excessive alcohol- or drug-use history, were recruited from the community and none from treatment centers. Disruption of microstructural integrity may require greater and more intense alcohol exposure in a larger sample of youth than examined herein. Further, although TBSS has the advantage of surveying white matter of the entire brain, modest compromise of fiber organization might be below detection with TBSS, which is based on tracking the highest FA values along the white matter skeleton. Larger subject samples would also be required to identify shifts in the age of the maximum regressed FA mean values related to excessive alcohol consumption.

Author Manuscript

Another consideration is the plasticity of brain fiber integrity with respect to development and trauma (Dennis et al., 2014; Peters and Sethares, 2003). If, for example, hazardous or binge drinking does exert an untoward effect on white matter microstructure, disruption might require examination soon after multiple, binge episodes. In support of this speculation is a controlled, longitudinal DTI study of a rodent model of binge drinking (Pfefferbaum et al., 2015a). Rats were exposed to 4 days of alcohol binge by oral gavage and underwent DTI before alcohol exposure, immediately following the 4-day binge, and after one week of recovery. Whereas control rats showed no FA differences across the 3 scanning sessions, the alcohol-exposed rats showed a significant decline in FA from DTI 1 to DTI 2, succeeded by a return to normal FA following a week of no alcohol.

Limitations, considerations, and conclusions

Inferences about developmental patterns must be made cautiously given the cross-sectional nature of these data and the limited age range. Confirmation of the patterns of the age associated with the highest regressed FA mean values awaits the longitudinal arms of the NCANDA study and higher-order diffusivity measures, which were outside of the foci of this paper. In accordance with the literature (Fischer et al., 2012; Jahanshad et al., 2013; Teipel et al., 2011; Zhu et al., 2011) the present analysis identified significant scanner manufacturer differences influencing quantification of the DTI data. Critically, we successful used travelling human phantom data to correct for these differences. As also noted by (Bartsch et al., 2014; Kochunov et al., 2015), harmonization of data is an essential step in ensuring that data collected across multiple sites and systems are equivalent, thereby enabling quantification on a common metric. Further, human phantom data will also be invaluable for harmonization of longitudinal data.

In conclusion, our cross-sectional analysis of DTI data from a large cohort of adolescents supports the concept that regional heterochronicity characterizes neurodevelopmental patterns of white matter fiber systems. Indeed, evidence was forthcoming with respect to asynchronous development of association fibers that connect cortical brain regions supporting high-order, cognitive functions. The continuing development of fiber bundles suggested herein may render them vulnerable to environmental insult, including hazardous drinking. This apparent plasticity noted in white matter microstructure might also enable speedy recovery of fiber system mildly damaged by such insult.

Supplementary Material

Refer to Web version on PubMed Central for supplementary material.

Acknowledgment

REFERENCES

Akshoomoff N, Newman E, Thompson WK, McCabe C, Bloss CS, Chang L, Amaral DG, Casey BJ, Ernst TM, Frazier JA, Gruen JR, Kaufmann WE, Kenet T, Kennedy DN, Libiger O, Mostofsky S, Murray SS, Sowell ER, Schork N, Dale AM, Jernigan TL. The NIH Toolbox Cognition Battery: results from a large normative developmental sample (PING). Neuropsychology. 2014; 28:1–10. [PubMed: 24219608]

Asato MR, Terwilliger R, Woo J, Luna B. White matter development in adolescence: a DTI study. Cereb Cortex. 2010; 20:2122–2131. [PubMed: 20051363]

Barnea-Goraly N, Menon V, Eckert M, Tamm L, Bammer R, Karchemskiy A, Dant CC, Reiss AL. White matter development during childhood and adolescence: a cross-sectional diffusion tensor imaging study. Cereb Cortex. 2005; 15:1848–1854. [PubMed: 15758200]

Barral J, Debu B, Rival C. Developmental changes in unimanual and bimanual aiming movements. Dev Neuropsychol. 2006; 29:415, 429. [PubMed: 16671859]

Bartsch H, Thompson WK, Jernigan TL, Dale AM. A web-portal for interactive data exploration, visualization, and hypothesis testing. Front Neuroinform. 2014; 8:25. [PubMed: 24723882]

Basser PJ, Pierpaoli C. Microstructural and physiological features of tissues elucidated by quantitative diffusion tensor MRI. Journal of Magnetic Resonance. Series B. 1996; 111:209, 219. [PubMed: 8661285]

Bava S, Boucquey V, Goldenberg D, Thayer RE, Ward M, Jacobus J, Tapert SF. Sex differences in adolescent white matter architecture. Brain Res. 2011; 1375:41–48. [PubMed: 21172320]

Bava S, Jacobus J, Mahmood O, Yang TT, Tapert SF. Neurocognitive correlates of white matter quality in adolescent substance users. Brain Cogn. 2010a; 72:347–354. [PubMed: 19932550]

Bava S, Jacobus J, Thayer RE, Tapert SF. Longitudinal changes in white matter integrity among adolescent substance users. Alcohol Clin Exp Res. 2013; 37(Suppl 1):E181–189. [PubMed: 23240741]

Bava S, Thayer R, Jacobus J, Ward M, Jernigan TL, Tapert SF. Longitudinal characterization of white matter maturation during adolescence. Brain Res. 2010b; 1327:38–46. [PubMed: 20206151]

Beaulieu C. The basis of anisotropic water diffusion in the nervous system - a technical review. NMR in Biomedicine. 2002; 15:435–455. [PubMed: 12489094]

Bodammer N, Kaufmann J, Kanowski M, Tempelmann C. Eddy current correction in diffusion-weighted imaging using pairs of images acquired with opposite diffusion gradient polarity. Magnetic Resonance in Medicine. 2004; 51:188–193. [PubMed: 14705060]

Brown SA, Brumback T, Tomlinson K, Cummins K, Thompson WK, Nagel BJ, De Bellis MD, Hooper SR, Clark DB, Chung T, Hasler BP, Colrain IM, Baker FC, Prouty D, Pfefferbaum A, Sullivan EV, Pohl KM, Rohlfing T, Nichols BN, Chu W, Tapert SF. The National Consortium on Alcohol and NeuroDevelopment in Adolescence (NCANDA): A multi-site study of adolescent development and substance use. Journal of Studies on Alcohol and Drugs. 2015; 76:895–908. [PubMed: 26562597]

Brown TT, Kuperman JM, Chung Y, Erhart M, McCabe C, Hagler DJ Jr. Venkatraman VK, Akshoomoff N, Amaral DG, Bloss CS, Casey BJ, Chang L, Ernst TM, Frazier JA, Gruen JR, Kaufmann WE, Kenet T, Kennedy DN, Murray SS, Sowell ER, Jernigan TL, Dale AM. Neuroanatomical assessment of biological maturity. Curr Biol. 2012; 22:1693–1698. [PubMed: 22902750]

Cancelliere A, Mangano FT, Air EL, Jones BV, Altaye M, Rajagopal A, Holland SK, Hertzler DA 2nd, Yuan W. DTI values in key white matter tracts from infancy through adolescence. AJNR Am J Neuroradiol. 2013; 34:1443–1449. [PubMed: 23370472]

Chen CH, Fiecas M, Gutierrez ED, Panizzon MS, Eyler LT, Vuoksimaa E, Thompson WK, Fennema-Notestine C, Hagler DJ Jr. Jernigan TL, Neale MC, Franz CE, Lyons MJ, Fischl B, Tsuang MT, Dale AM, Kremen WS. Genetic topography of brain morphology. Proc Natl Acad Sci U S A. 2013; 110:17089–17094. [PubMed: 24082094]

Chugani HT, Phelps ME, Mazziotta JC. Positron emission tomography study of human brain functional development. Annals of Neurology. 1987; 22:487–497. [PubMed: 3501693]

Cook, PA.; Bai, Y.; Nedjati-Gilani, S.; Seunarine, KK.; Hall, MG.; Parker, GJ.; Alexander, DC. Camino: Open-source diffusion-MRI reconstruction and processing; 14th Scientific Meeting of the International Society for Magnetic Resonance in Medicine; Seattle, WA. 2006; p. 2759

de Boer BJ, Peper CE, Beek PJ. Development of temporal and spatial bimanual coordination during childhood. Motor Control. 2012; 16:537–559. [PubMed: 23162066]

Dennis M, Spiegler BJ, Simic N, Sinopoli KJ, Wilkinson A, Yeates KO, Taylor HG, Bigler ED, Fletcher JM. Functional plasticity in childhood brain disorders: when, what, how, and whom to assess. Neuropsychol Rev. 2014; 24:389–408. [PubMed: 24821533]

Dick AS, Tremblay P. Beyond the arcuate fasciculus: consensus and controversy in the connectional anatomy of language. Brain. 2012; 135:3529–3550. [PubMed: 23107648]

Elofson J, Gongvatana W, Carey KB. Alcohol use and cerebral white matter compromise in adolescence. Addict Behav. 2013; 38:2295–2305. [PubMed: 23583835]

Farbota KD, Bendlin BB, Alexander AL, Rowley HA, Dempsey RJ, Johnson SC. Longitudinal diffusion tensor imaging and neuropsychological correlates in traumatic brain injury patients. Front Hum Neurosci. 2014; 6:160. [PubMed: 22723773]

Feinberg I. Changes in sleep cycle patterns with age. Journal of Psychiatric Research. 1974; 10:283–306. [PubMed: 4376564]

Feinberg I. Extensive brain development period offers insights to illnesses. The Psychiatric Times Medicine & Behavior. 1990:12–16.

Feinberg I, Thode HC, Chugani HT, March JD. Gamma distribution model describes maturational curves for delta wave amplitude, cortical metabolic rate and synaptic density. Journal of Theoretical Biology. 1990; 142:149–161. [PubMed: 2161971]

Fischer FU, Scheurich A, Wegrzyn M, Schermuly I, Bokde AL, Kloppel S, Pouwels PJ, Teipel S, Yakushev I, Fellgiebel A. Automated tractography of the cingulate bundle in Alzheimer's disease: a multicenter DTI study. J Magn Reson Imaging. 2012; 36:84–91. [PubMed: 22359373]

Fryer SL, Frank LR, Spadoni AD, Theilmann RJ, Nagel BJ, Schweinsburg AD, Tapert SF. Microstructural integrity of the corpus callosum linked with neuropsychological performance in adolescents. Brain Cogn. 2008

Giedd JN, Raznahan A, Alexander-Bloch A, Schmitt E, Gogtay N, Rapoport JL. Child psychiatry branch of the National Institute of Mental Health longitudinal structural magnetic resonance imaging study of human brain development. Neuropsychopharmacology. 2014; 40:43–49. [PubMed: 25195638]

Giorgio A, Watkins KE, Chadwick M, James S, Winmill L, Douaud G, De Stefano N, Matthews PM, Smith SM, Johansen-Berg H, James AC. Longitudinal changes in grey and white matter during adolescence. Neuroimage. 2010; 49:94–103. [PubMed: 19679191]

Giorgio A, Watkins KE, Douaud G, James AC, James S, De Stefano N, Matthews PM, Smith SM, Johansen-Berg H. Changes in white matter microstructure during adolescence. Neuroimage. 2008; 39:52–61. [PubMed: 17919933]

Glover GH, Mueller BA, Turner JA, van Erp TG, Liu TT, Greve DN, Voyvodic JT, Rasmussen J, Brown GG, Keator DB, Calhoun VD, Lee HJ, Ford JM, Mathalon DH, Diaz M, O'Leary DS, Gadde S, Preda A, Lim KO, Wible CG, Stern HS, Belger A, McCarthy G, Ozyurt B, Potkin SG. Function biomedical informatics research network recommendations for prospective multicenter functional MRI studies. J Magn Reson Imaging. 2012; 36:39–54. [PubMed: 22314879]

Groves AR, Smith SM, Fjell AM, Tamnes CK, Walhovd KB, Douaud G, Woolrich MW, Westlye LT. Benefits of multi-modal fusion analysis on a large-scale dataset: life-span patterns of inter-subject variability in cortical morphometry and white matter microstructure. Neuroimage. 2012; 63:365–380. [PubMed: 22750721]

Harris PA, Taylor R, Thielke R, Payne J, Gonzalez N, Conde JG. Research electronic data capture (REDCap) - A metadata-driven methodology and workflow process for providing translational research informatics support. J Biomed Inform. 2009; 42:377–381. [PubMed: 18929686]

Hasan KM, Kamali A, Abid H, Kramer LA, Fletcher JM, Ewing-Cobbs L. Quantification of the spatiotemporal microstructural organization of the human brain association, projection and commissural pathways across the lifespan using diffusion tensor tractography. Brain Struct Funct. 2010; 214:361–373. [PubMed: 20127357]

Hasan KM, Kamali A, Iftikhar A, Kramer LA, Papanicolaou AC, Fletcher JM, Ewing-Cobbs L. Diffusion tensor tractography quantification of the human corpus callosum fiber pathways across the lifespan. Brain Res. 2009; 1249:91–100. [PubMed: 18996095]

Hastie T, Tibshirani R. Generalized additive models (with DIscussion). Statistical Science. 1986; 1:297–318.

Hastie T, Tibshirani R. Exploring the nature of covariate effects in the proportional hazards model. Biometrics. 1990; 46:1005–1016. [PubMed: 1964808]

Herting MM, Colby JB, Sowell ER, Nagel BJ. White matter connectivity and aerobic fitness in male adolescents. Dev Cogn Neurosci. 2014; 7:65–75. [PubMed: 24333926]

Herting MM, Maxwell EC, Irvine C, Nagel BJ. The impact of sex, puberty, and hormones on white matter microstructure in adolescents. Cereb Cortex. 2012; 22:1979–1992. [PubMed: 22002939]

Hill SY, Terwilliger R, McDermott M. White matter microstructure, alcohol exposure, and familial risk for alcohol dependence. Psychiatry Res. 2013; 212:43–53. [PubMed: 23473988]

Hoeft F, McCandliss BD, Black JM, Gantman A, Zakerani N, Hulme C, Lyytinen H, Whitfield-Gabrieli S, Glover GH, Reiss AL, Gabrieli JD. Neural systems predicting long-term outcome in dyslexia. Proc Natl Acad Sci U S A. 2011; 108:361–366. [PubMed: 21173250]

Hogstrom LJ, Westlye LT, Walhovd KB, Fjell AM. The structure of the cerebral cortex across adult life: age-related patterns of surface area, thickness, and gyrification. Cereb Cortex. 2013; 23:2521–2530. [PubMed: 22892423]

Holland D, Kuperman JM, Dale AM. Efficient correction of inhomogeneous static magnetic field-induced distortion in Echo Planar Imaging. Neuroimage. 2010; 50:175–183. [PubMed: 19944768]

Hua K, Oishi K, Zhang J, Wakana S, Yoshioka T, Zhang W, Akhter KD, Li X, Huang H, Jiang H, van Zijl P, Mori S. Mapping of functional areas in the human cortex based on connectivity through association fibers. Cereb Cortex. 2009; 19:1889–1895. [PubMed: 19068488]

Huttenlocher PR. Synaptic density in human frontal cortex: Developmental changes and effects of aging. Brain Research. 1979; 163:195–205. [PubMed: 427544]

Huttenlocher PR, Dabholkar AS. Regional differences in synaptogenesis in human cerebral cortex. J Comp Neurol. 1997; 387:167–178. [PubMed: 9336221]

Iglesias JE, Liu CY, Thompson PM, Tu Z. Robust brain extraction across datasets and comparison with publicly available methods. IEEE Trans Med Imaging. 2011; 30:1617–1634. [PubMed: 21880566]

Jacobs HI, Gronenschild EH, Evers EA, Ramakers IH, Hofman PA, Backes WH, Jolles J, Verhey FR, Van Boxtel MP. Visuospatial processing in early Alzheimer's disease: a multimodal neuroimaging study. Cortex. 2015; 64:394–406. [PubMed: 22342463]

Jacobus J, McQueeny T, Bava S, Schweinsburg BC, Frank LR, Yang TT, Tapert SF. White matter integrity in adolescents with histories of marijuana use and binge drinking. Neurotoxicol Teratol. 2009; 31:349–355. [PubMed: 19631736]

Jacobus J, Squeglia LM, Bava S, Tapert SF. White matter characterization of adolescent binge drinking with and without co-occurring marijuana use: a 3-year investigation. Psychiatry Res. 2013; 214:374–381. [PubMed: 24139957]

Jahanshad N, Kochunov PV, Sprooten E, Mandl RC, Nichols TE, Almasy L, Blangero J, Brouwer RM, Curran JE, de Zubicaray GI, Duggirala R, Fox PT, Hong LE, Landman BA, Martin NG, McMahon KL, Medland SE, Mitchell BD, Olvera RL, Peterson CP, Starr JM, Sussmann JE, Toga AW, Wardlaw JM, Wright MJ, Hulshoff Pol HE, Bastin ME, McIntosh AM, Deary IJ, Thompson PM, Glahn DC. Multi-site genetic analysis of diffusion images and voxelwise heritability analysis: a pilot project of the ENIGMA-DTI working group. Neuroimage. 2013; 81:455–469. [PubMed: 23629049]

Jones DK. The effect of gradient sampling schemes on measures derived from diffusion tensor MRI: a Monte Carlo study. Magnetic Resonance in Medicine. 2004; 51:807–815. [PubMed: 15065255]

Jovicich J, Marizzoni M, Bosch B, Bartres-Faz D, Arnold J, Benninghoff J, Wiltfang J, Roccatagliata L, Picco A, Nobili F, Blin O, Bombois S, Lopes R, Bordet R, Chanoine V, Ranjeva JP, Didic M, Gros-Dagnac H, Payoux P, Zoccatelli G, Alessandrini F, Beltramello A, Bargallo N, Ferretti A, Caulo M, Aiello M, Ragucci M, Soricelli A, Salvadori N, Tarducci R, Floridi P, Tsolaki M, Constantinidis M, Drevelegas A, Rossini PM, Marra C, Otto J, Reiss-Zimmermann M, Hoffmann

KT, Galluzzi S, Frisoni GB, PharmaCog C. Multisite longitudinal reliability of tract-based spatial statistics in diffusion tensor imaging of healthy elderly subjects. Neuroimage. 2014; 101:390–403. [PubMed: 25026156]

Kochunov P, Jahanshad N, Marcus D, Winkler A, Sprooten E, Nichols TE, Wright SN, Hong LE, Patel B, Behrens T, Jbabdi S, Andersson J, Lenglet C, Yacoub E, Moeller S, Auerbach E, Ugurbil K, Sotiropoulos SN, Brouwer RM, Landman B, Lemaitre H, den Braber A, Zwiers MP, Ritchie S, van Hulzen K, Almasy L, Curran J, deZubicaray GI, Duggirala R, Fox P, Martin NG, McMahon KL, Mitchell B, Olvera RL, Peterson C, Starr J, Sussmann J, Wardlaw J, Wright M, Boomsma DI, Kahn R, de Geus EJ, Williamson DE, Hariri A, van 't Ent D, Bastin ME, McIntosh A, Deary IJ, Hulshoff Pol HE, Blangero J, Thompson PM, Glahn DC, Van Essen DC. Heritability of fractional anisotropy in human white matter: a comparison of Human Connectome Project and ENIGMA-DTI data. Neuroimage. 2015; 111:300–311. [PubMed: 25747917]

Kochunov P, Jahanshad N, Sprooten E, Nichols TE, Mandl RC, Almasy L, Booth T, Brouwer RM, Curran JE, de Zubicaray GI, Dimitrova R, Duggirala R, Fox PT, Hong LE, Landman BA, Lemaitre H, Lopez LM, Martin NG, McMahon KL, Mitchell BD, Olvera RL, Peterson CP, Starr JM, Sussmann JE, Toga AW, Wardlaw JM, Wright MJ, Wright SN, Bastin ME, McIntosh AM, Boomsma DI, Kahn RS, den Braber A, de Geus EJ, Deary IJ, Hulshoff Pol HE, Williamson DE, Blangero J, van 't Ent D, Thompson PM, Glahn DC. Multi-site study of additive genetic effects on fractional anisotropy of cerebral white matter: Comparing meta and megaanalytical approaches for data pooling. Neuroimage. 2014; 95:136–150. [PubMed: 24657781]

Koob GF. Brain stress systems in the amygdala and addiction. Brain Research. 2009

Kreilkamp BA, Zaca D, Papinutto N, Jovicich J. Retrospective head motion correction approaches for diffusion tensor imaging: Effects of preprocessing choices on biases and reproducibility of scalar diffusion metrics. J Magn Reson Imaging. 2015

Lebel C, Gee M, Camicioli R, Wieler M, Martin W, Beaulieu C. Diffusion tensor imaging of white matter tract evolution over the lifespan. Neuroimage. 2012; 60:340–352. [PubMed: 22178809]

Lebel C, Walker L, Leemans A, Phillips L, Beaulieu C. Microstructural maturation of the human brain from childhood to adulthood. Neuroimage. 2008; 40:1044–1055. [PubMed: 18295509]

Lenroot RK, Gogtay N, Greenstein DK, Wells EM, Wallace GL, Clasen LS, Blumenthal JD, Lerch J, Zijdenbos AP, Evans AC, Thompson PM, Giedd JN. Sexual dimorphism of brain developmental trajectories during childhood and adolescence. Neuroimage. 2007; 36:1065–1073. [PubMed: 17513132]

Liu X, Zhu T, Gu T, Zhong J. Optimization of in vivo high-resolution DTI of non-human primates on a 3T human scanner. Methods. 2010; 50:205–213. [PubMed: 19577649]

MacArthur GJ, Smith MC, Melotti R, Heron J, Macleod J, Hickman M, Kipping RR, Campbell R, Lewis G. Patterns of alcohol use and multiple risk behaviour by gender during early and late adolescence: the ALSPAC cohort. J Public Health (Oxf). 2012; 34(Suppl 1):i20–30. [PubMed: 22363027]

Marion SD, Kilian SC, Naramor TL, Brown WS. Normal development of bimanual coordination: visuomotor and interhemispheric contributions. Dev Neuropsychol. 2003; 23:399–421. [PubMed: 12740193]

Martino J, De Lucas EM. Subcortical anatomy of the lateral association fascicles of the brain: A review. Clin Anat. 2014; 27:563–569. [PubMed: 24453050]

McKay DR, Knowles EE, Winkler AA, Sprooten E, Kochunov P, Olvera RL, Curran JE, Kent JW Jr. Carless MA, Goring HH, Dyer TD, Duggirala R, Almasy L, Fox PT, Blangero J, Glahn DC. Influence of age, sex and genetic factors on the human brain. Brain Imaging Behav. 2014; 8:143–152. [PubMed: 24297733]

Menjot de Champfleur N, Lima Maldonado I, Moritz-Gasser S, Machi P, Le Bars E, Bonafe A, Duffau H. Middle longitudinal fasciculus delineation within language pathways: a diffusion tensor imaging study in human. Eur J Radiol. 2013; 82:151–157. [PubMed: 23084876]

Mori, S.; Wakana, S.; Nagae-Poetscher, LM.; Van Zijl, PMC. An Atlas of Human White Matter. Elsevier B.V.; Amsterdam, the Netherlands: 2005.

Muetzel RL, Collins PF, Mueller BA, A MS, Lim KO, Luciana M. The development of corpus callosum microstructure and associations with bimanual task performance in healthy adolescents. Neuroimage. 2008; 39:1918–1925. [PubMed: 18060810]

Nichols BN, Pohl KM. Neuroinformatics Software Applications Supporting Electronic Data Capture, Management, and Sharing for the Neuroimaging Community. Neuropsychol Rev. 2015

Nowrangi MA, Lyketsos CG, Leoutsakos JM, Oishi K, Albert M, Mori S, Mielke MM. Longitudinal, region-specific course of diffusion tensor imaging measures in mild cognitive impairment and Alzheimer's disease. Alzheimers Dement. 2013; 9:519–528. [PubMed: 23245561]

O'Sullivan M, Jones D, Summers P, Morris R, Williams S, Markus H. Evidence for cortical "disconnection" as a mechanism of age-related cognitive decline. Neurology. 2001; 57:632–638. [PubMed: 11524471]

Ostby Y, Tamnes CK, Fjell AM, Walhovd KB. Morphometry and connectivity of the fronto-parietal verbal working memory network in development. Neuropsychologia. 2011; 49:3854–3862. [PubMed: 22001853]

Paldino MJ, Hedges K, Zhang W. Independent contribution of individual white matter pathways to language function in pediatric epilepsy patients. Neuroimage Clin. 2014; 6:327–332. [PubMed: 25379446]

Papinutto ND, Maule F, Jovicich J. Reproducibility and biases in high field brain diffusion MRI: An evaluation of acquisition and analysis variables. Magn Reson Imaging. 2013; 31:827–839. [PubMed: 23623031]

Paus T. Growth of white matter in the adolescent brain: myelin or axon? Brain Cogn. 2010; 72:26–35. [PubMed: 19595493]

Perrin JS, Herve PY, Leonard G, Perron M, Pike GB, Pitiot A, Richer L, Veillette S, Pausova Z, Paus T. Growth of white matter in the adolescent brain: role of testosterone and androgen receptor. J Neurosci. 2008; 28:9519–9524. [PubMed: 18799683]

Peters A, Sethares C. Is there remyelination during aging of the primate central nervous system? Journal of Comparative Neurology. 2003; 460:238–254. [PubMed: 12687688]

Peters BD, Szeszko PR, Radua J, Ikuta T, Gruner P, DeRosse P, Zhang JP, Giorgio A, Qiu D, Tapert SF, Brauer J, Asato MR, Khong PL, James AC, Gallego JA, Malhotra AK. White matter development in adolescence: diffusion tensor imaging and meta-analytic results. Schizophr Bull. 2012; 38

Pfefferbaum A, Rogosa DA, Rosenbloom MJ, Chu W, Sassoon SA, Kemper CA, Deresinski S, Rohlfing T, Zahr NM, Sullivan EV. Accelerated aging of selective brain structures in human immunodeficiency virus infection: a controlled, longitudinal magnetic resonance imaging study. Neurobiol Aging. 2014; 35:1755–1768. [PubMed: 24508219]

Pfefferbaum A, Rohlfing T, Rosenbloom MJ, Chu W, Colrain IM, Sullivan EV. Variation in longitudinal trajectories of regional brain volumes of healthy men and women (ages 10 to 85 years) measured with atlas-based parcellation of MRI. NeuroImage. 2013; 65:176–193. [PubMed: 23063452]

Pfefferbaum A, Sullivan EV. Microstructural but not macrostructural disruption of white matter in women with chronic alcoholism. NeuroImage. 2002; 15:708–718. [PubMed: 11848714]

Pfefferbaum A, Zahr NM, Mayer D, Rohlfing T, Sullivan EV. Dynamic responses of selective brain white matter fiber tracts to binge alcohol and recovery in the rat. PLoS One. 2015a; 10:e0124885. [PubMed: 25894968]

Pfefferbaum D, Rohlfing T, Poh KM, Lane B, Weiwei C, Nichols BN, Brown SA, Tapert SF, Cummins K, Thompson WK, Brumback T, Meloy MJ, Jernigan TL, Dale AM, Colrain IM, Baker FC, Prouty D, De Bellis MD, Voyvodic JT, Clark DB, Luna B, Chung T, Nagel BJ, Sullivan EV. Adolescent development of cortical and white matter structure in the NCANDA sample: Role of sex, ethnicity, puberty, and alcohol drinking. Cerebral Cortex. 2015b Epub Sep 26.

Qiu D, Tan LH, Zhou K, Khong PL. Diffusion tensor imaging of normal white matter maturation from late childhood to young adulthood: voxel-wise evaluation of mean diffusivity, fractional anisotropy, radial and axial diffusivities, and correlation with reading development. Neuroimage. 2008; 41:223–232. [PubMed: 18395471]

Raz N, Ghisletta P, Rodrigue KM, Kennedy KM, Lindenberger U. Trajectories of brain aging in middle-aged and older adults: regional and individual differences. Neuroimage. 2010; 51:501–511. [PubMed: 20298790]

Raznahan A, Greenstein D, Lee NR, Clasen LS, Giedd JN. Prenatal growth in humans and postnatal brain maturation into late adolescence. Proc Natl Acad Sci U S A. 2012; 109:11366–11371. [PubMed: 22689983]

Raznahan A, Lee Y, Stidd R, Long R, Greenstein D, Clasen L, Addington A, Gogtay N, Rapoport JL, Giedd JN. Longitudinally mapping the influence of sex and androgen signaling on the dynamics of human cortical maturation in adolescence. Proceedings of the National Academy of Sciences of the United States of America. 2010; 107:16988–16993. [PubMed: 20841422]

Rohlfing T, Cummins K, Henthorn T, Chu W, Nichols BN. N-CANDA data integration: anatomy of an asynchronous infrastructure for multi-site, multi-instrument longitudinal data capture. J Am Med Inform Assoc. 2014; 21:758–762. [PubMed: 24296908]

Rohlfing T, Maurer CR Jr. Bluemke DA, Jacobs MA. Volume-preserving nonrigid registration of MR breast images using free-form deformation with an incompressibility constraint. IEEE Transactions on Medical Imaging. 2003a; 22:730–741. [PubMed: 12872948]

Rohlfing, T.; Maurer, CR., Jr; Bluemke, DA.; Jacobs, MA. An Alternating-Constraints Algorithm for Volume-Preserving Non-Rigid Registration of Contrast-Enhanced MR Breast Images; Biomedical Image Registration -- Second International Workshop; WBIR, Philadelphia, PA. 2003b. p. 291-300.

Rohlfing T, Russakoff DB, Maurer CR Jr. Performance-Based Classifier Combination in Atlas-Based Image Segmentation Using Expectation-Maximization Parameter Estimation. IEEE Transactions on Medical Imaging. 2004; 23:983–994. [PubMed: 15338732]

Rohlfing T, Zahr NM, Sullivan EV, Pfefferbaum A. The SRI24 multi-channel atlas of normal adult human brain structure. Human Brain Mapping. 2010; 31:798–819. [PubMed: 20017133]

Ross RT. Dissociated loss of vibration, joint position and discriminatory tactile senses in disease of spinal cord and brain. Can J Neurol Sci. 1991; 18:312–320. [PubMed: 1913366]

Sadeghi N, Prastawa M, Fletcher PT, Vachet C, Wang B, Gilmore J, Gerig G. Multivariate Modeling of Longitudinal Mri in Early Brain Development with Confidence Measures. Proc IEEE Int Symp Biomed Imaging. 2013:1400–1403. [PubMed: 23959506]

Salat DH, Tuch DS, van der Kouwe AJ, Greve DN, Pappu V, Lee SY, Hevelone ND, Zaleta AK, Growdon JH, Corkin S, Fischl B, Rosas HD. White matter pathology isolates the hippocampal formation in Alzheimer's disease. Neurobiol Aging. 2010; 31:244–256. [PubMed: 18455835]

Schmahmann JD, Pandya DN. The complex history of the fronto-occipital fasciculus. J Hist Neurosci. 2007; 16:362–377. [PubMed: 17966054]

Schmitt JE, Neale MC, Fassassi B, Perez J, Lenroot RK, Wells EM, Giedd JN. The dynamic role of genetics on cortical patterning during childhood and adolescence. Proc Natl Acad Sci U S A. 2014; 111:6774–6779. [PubMed: 24753564]

Schneiderman JS, Buchsbaum MS, Haznedar MM, Hazlett EA, Brickman AM, Shihabuddin L, Brand JG, Torosjan Y, Newmark RE, Tang C, Aronowitz J, Paul-Odouard R, Byne W, Hof PR. Diffusion tensor anisotropy in adolescents and adults. Neuropsychobiology. 2007; 55:96–111. [PubMed: 17587876]

Shinoura N, Suzuki Y, Yamada R, Tabei Y, Saito K, Yagi K. Damage to the right superior longitudinal fasciculus in the inferior parietal lobe plays a role in spatial neglect. Neuropsychologia. 2009; 47:2600, 2603. [PubMed: 19465036]

Shinoura N, Yoshida M, Yamada R, Tabei Y, Saito K, Suzuki Y, Yagi K. Combined damage to the right hemispheric hand area in the primary motor and sensory area plays a critical role in motor hemineglect. Eur Neurol. 2010; 63:17–23. [PubMed: 19923840]

Simmonds DJ, Hallquist MN, Asato M, Luna B. Developmental stages and sex differences of white matter and behavioral development through adolescence: a longitudinal diffusion tensor imaging (DTI) study. Neuroimage. 2014; 92:356–368. [PubMed: 24384150]

Smith S. Fast robust automated brain extraction. Human Brain Mapping. 2002; 17:143–155. [PubMed: 12391568]

Smith SM, Jenkinson M, Johansen-Berg H, Rueckert D, Nichols TE, Mackay CE, Watkins KE, Ciccarelli O, Cader MZ, Matthews PM, Behrens TE. Tract-based spatial statistics: voxelwise analysis of multi-subject diffusion data. Neuroimage. 2006; 31:1487, 1505. [PubMed: 16624579]

Snook L, Paulson LA, Roy D, Phillips L, Beaulieu C. Diffusion tensor imaging of neurodevelopment in children and young adults. Neuroimage. 2005; 26:1164–1173. [PubMed: 15961051]

Sowell ER, Peterson BS, Kan E, Woods RP, Yoshii J, Bansal R, Xu D, Zhu H, Thompson PM, Toga AW. Sex differences in cortical thickness mapped in 176 healthy individuals between 7 and 87 years of age. Cereb Cortex. 2007; 17:1550–1560. [PubMed: 16945978]

Sowell ER, Thompson PM, Toga AW. Mapping changes in the human cortex throughout the span of life. Neuroscientist. 2004; 10:372–392. [PubMed: 15271264]

Squire LR, Zola-Morgan S. The medial temporal lobe memory system. Science. 1991; 253:1380–1386. [PubMed: 1896849]

Stiles J, Jernigan TL. The basics of brain development. Neuropsychol Rev. 2010; 20:327–348. [PubMed: 21042938]

Storsve AB, Fjell AM, Tamnes CK, Westlye LT, Overbye K, Aasland HW, Walhovd KB. Differential longitudinal changes in cortical thickness, surface area and volume across the adult life span: regions of accelerating and decelerating change. J Neurosci. 2014; 34:8488–8498. [PubMed: 24948804]

Sullivan EV. Compromised pontocerebellar and cerebellothalamocortical systems: speculations on their contributions to cognitive and motor impairment in nonamnesic alcoholism. Alcoholism: Clinical and Experimental Research. 2003; 27:1409–1419.

Sullivan EV, Brumback T, Tapert SF, Fama R, Prouty D, Brown SA, Cummins K, Thompson WK, Colrain IM, Baker FC, De Bellis MD, Hooper SR, Clark DB, Chung T, Nagel BJ, Nichols BN, Rohlfing T, Chu W, Pohl KM, Pfefferbaum A. Cognitive, Emotion Control, and Motor Performance of Adolescents in the NCANDA Study: Contributions From Alcohol Consumption, Age, Sex, Ethnicity, and Family History of Addiction. Neuropsychology. 2016

Swendsen J, Burstein M, Case B, Conway KP, Dierker L, He J, Merikangas KR. Use and abuse of alcohol and illicit drugs in US adolescents: results of the National Comorbidity Survey-Adolescent Supplement. Arch Gen Psychiatry. 2012; 69:390–398. [PubMed: 22474107]

Tamnes CK, Ostby Y, Fjell AM, Westlye LT, Due-Tonnessen P, Walhovd KB. Brain maturation in adolescence and young adulthood: regional age-related changes in cortical thickness and white matter volume and microstructure. Cereb Cortex. 2010a; 20:534–548. [PubMed: 19520764]

Tamnes CK, Ostby Y, Walhovd KB, Westlye LT, Due-Tonnessen P, Fjell AM. Intellectual abilities and white matter microstructure in development: a diffusion tensor imaging study. Hum Brain Mapp. 2010b; 31:1609–1625. [PubMed: 20162594]

Teipel SJ, Reuter S, Stieltjes B, Acosta-Cabronero J, Ernemann U, Fellgiebel A, Filippi M, Frisoni G, Hentschel F, Jessen F, Kloppel S, Meindl T, Pouwels PJ, Hauenstein KH, Hampel H. Multicenter stability of diffusion tensor imaging measures: a European clinical and physical phantom study. Psychiatry Res. 2011; 194:363–371. [PubMed: 22078796]

Toga AW, Thompson PM, Sowell ER. Mapping brain maturation. Trends Neurosci. 2006; 29:148–159. [PubMed: 16472876]

Treit S, Lebel C, Baugh L, Rasmussen C, Andrew G, Beaulieu C. Longitudinal MRI reveals altered trajectory of brain development during childhood and adolescence in fetal alcohol spectrum disorders. J Neurosci. 2013; 33:10098–10109. [PubMed: 23761905]

Vandekar SN, Shinohara RT, Raznahan A, Roalf DR, Ross M, DeLeo N, Ruparel K, Verma R, Wolf DH, Gur RC, Gur RE, Satterthwaite TD. Topologically dissociable patterns of development of the human cerebral cortex. J Neurosci. 2015; 35:599–609. [PubMed: 25589754]

Vestergaard M, Madsen KS, Baare WF, Skimminge A, Ejersbo LR, Ramsoy TZ, Gerlach C, Akeson P, Paulson OB, Jernigan TL. White matter microstructure in superior longitudinal fasciculus associated with spatial working memory performance in children. J Cogn Neurosci. 2011; 23:2135–2146. [PubMed: 20964591]

Wang Y, Adamson C, Yuan W, Altaye M, Rajagopal A, Byars AW, Holland SK. Sex differences in white matter development during adolescence: a DTI study. Brain Res. 2012; 1478:1–15. [PubMed: 22954903]

White T, Magnotta VA, Bockholt HJ, Williams S, Wallace S, Ehrlich S, Mueller BA, Ho BC, Jung RE, Clark VP, Lauriello J, Bustillo JR, Schulz SC, Gollub RL, Andreasen NC, Calhoun VD, Lim

KO. Global white matter abnormalities in schizophrenia: a multisite diffusion tensor imaging study. Schizophr Bull. 2011; 37:222–232. [PubMed: 19770491]

Wood SN. Low-rank scale-invariant tensor product smooths for generalized additive mixed models. Biometrics. 2006; 62:1025–1036. [PubMed: 17156276]

Wood SN. Fast stable restricted maximum likelihood and marginal likelihood estimation of semiparametric generalized linear modelsFast stable restricted maximum likelihood and marginal likelihood estimation of semiparametric generalized linear models. Journal of the Royal Statistical Society (B). 2011; 73:3–36.

Yeatman JD, Wandell BA, Mezer AA. Lifespan maturation and degeneration of human brain white matter. Nat Commun. 2014; 5:4932. [PubMed: 25230200]

Yendiki A, Koldewyn K, Kakunoori S, Kanwisher N, Fischl B. Spurious group differences due to head motion in a diffusion MRI study. Neuroimage. 2013; 88C:79–90. [PubMed: 24269273]

Zhang M, Chen C, Xue G, Lu ZL, Mei L, Xue H, Wei M, He Q, Li J, Dong Q. Language-general and -specific white matter microstructural bases for reading. Neuroimage. 2014; 98:435–441. [PubMed: 24814214]

Zhu T, Hu R, Qiu X, Taylor M, Tso Y, Yiannoutsos C, Navia B, Mori S, Ekholm S, Schifitto G, Zhong J. Quantification of accuracy and precision of multi-center DTI measurements: a diffusion phantom and human brain study. Neuroimage. 2011; 56:1398–1411. [PubMed: 21316471]

Zhuang L, Sachdev PS, Trollor JN, Reppermund S, Kochan NA, Brodaty H, Wen W. Microstructural white matter changes, not hippocampal atrophy, detect early amnestic mild cognitive impairment. PLoS One. 2013; 8:e58887. [PubMed: 23516569]
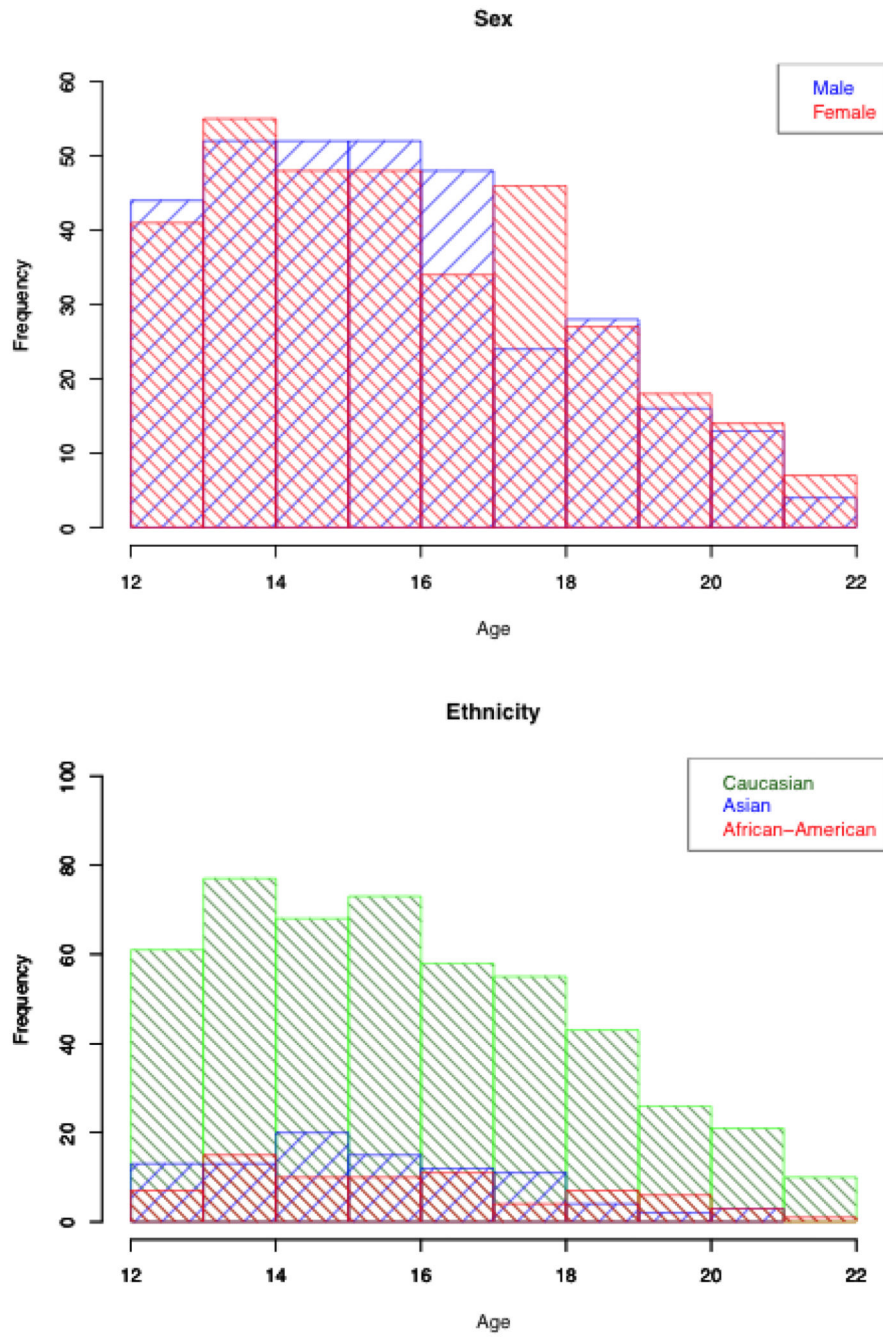
Figure 1.
Frequency histograms of sex by age (top) and ethnicity by age (bottom)
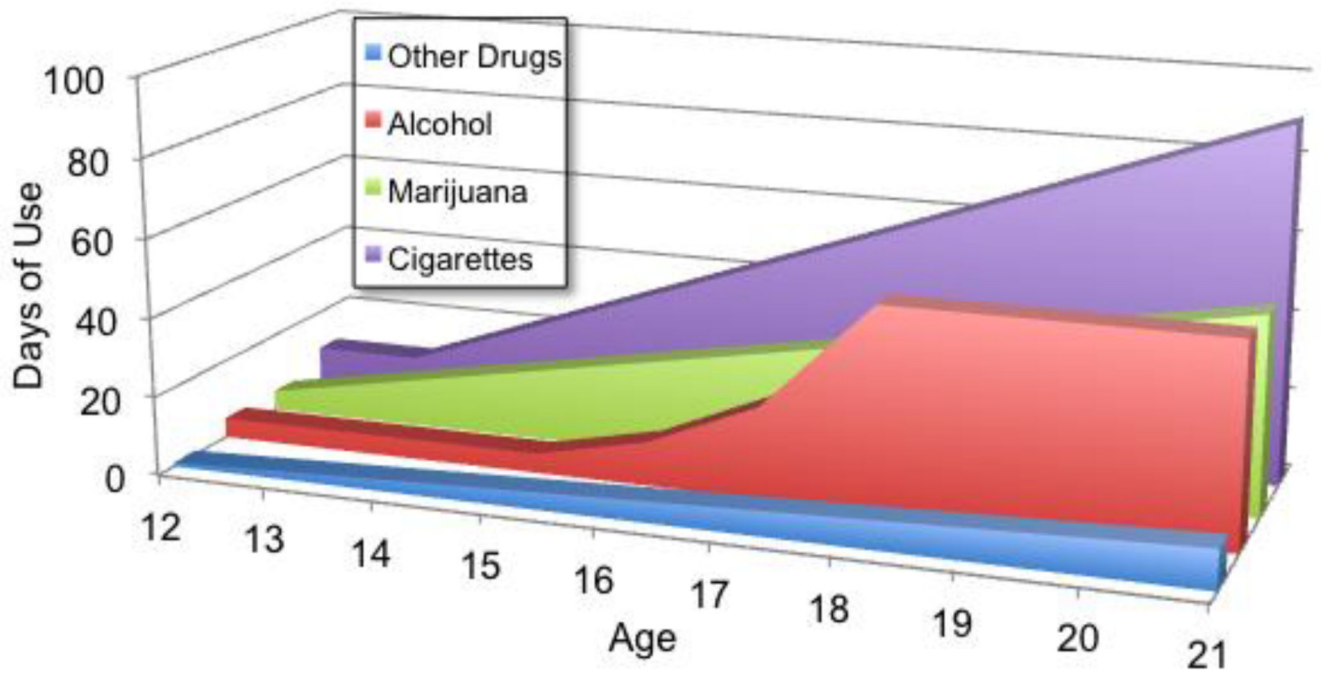
Figure 2.
Age-dependent criteria for alcohol, marijuana, cigarettes, and other drugs for the no/low-drinking NCANDA group. The blue and white figures indicate the maximum number of drinks allowable in one day by sex and age.
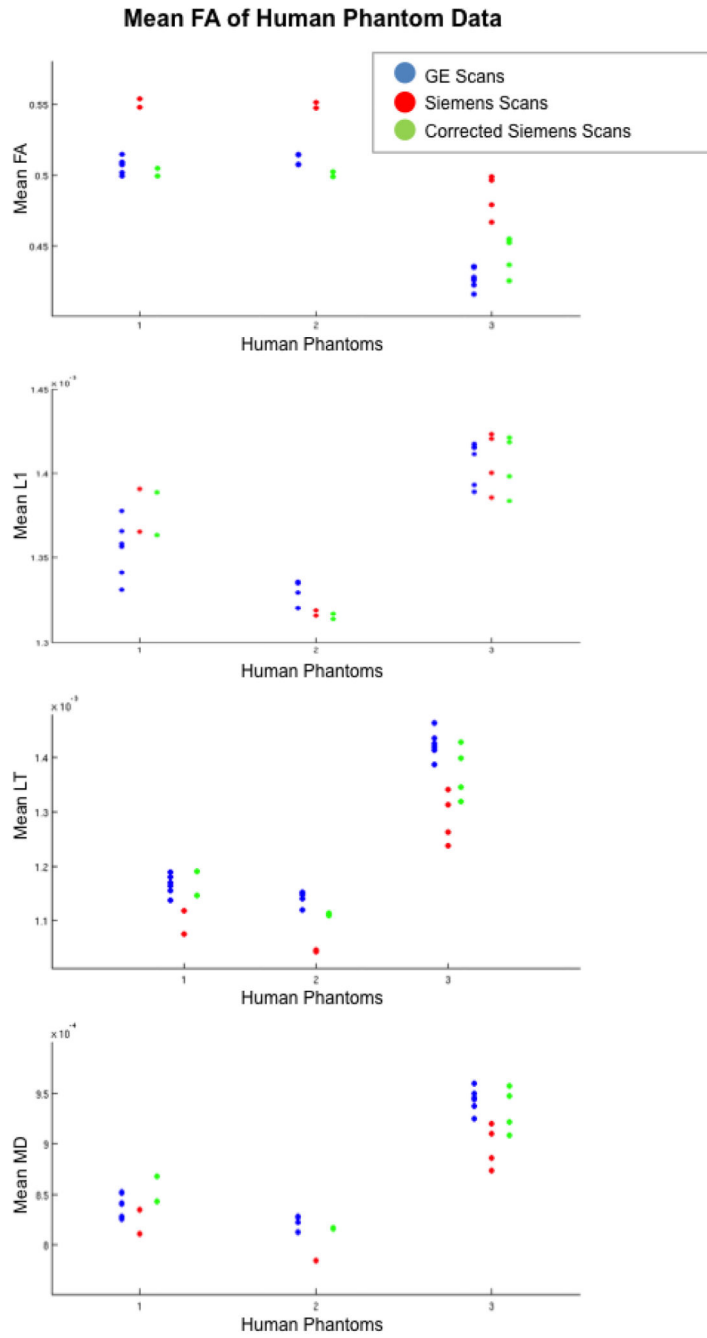
Figure 3.
Mean FA of the brain of 27 human phantom visits with the x-axis listing the three subjects by age. For each subject, the clusters associated with the scanners are clearly separated from each other.
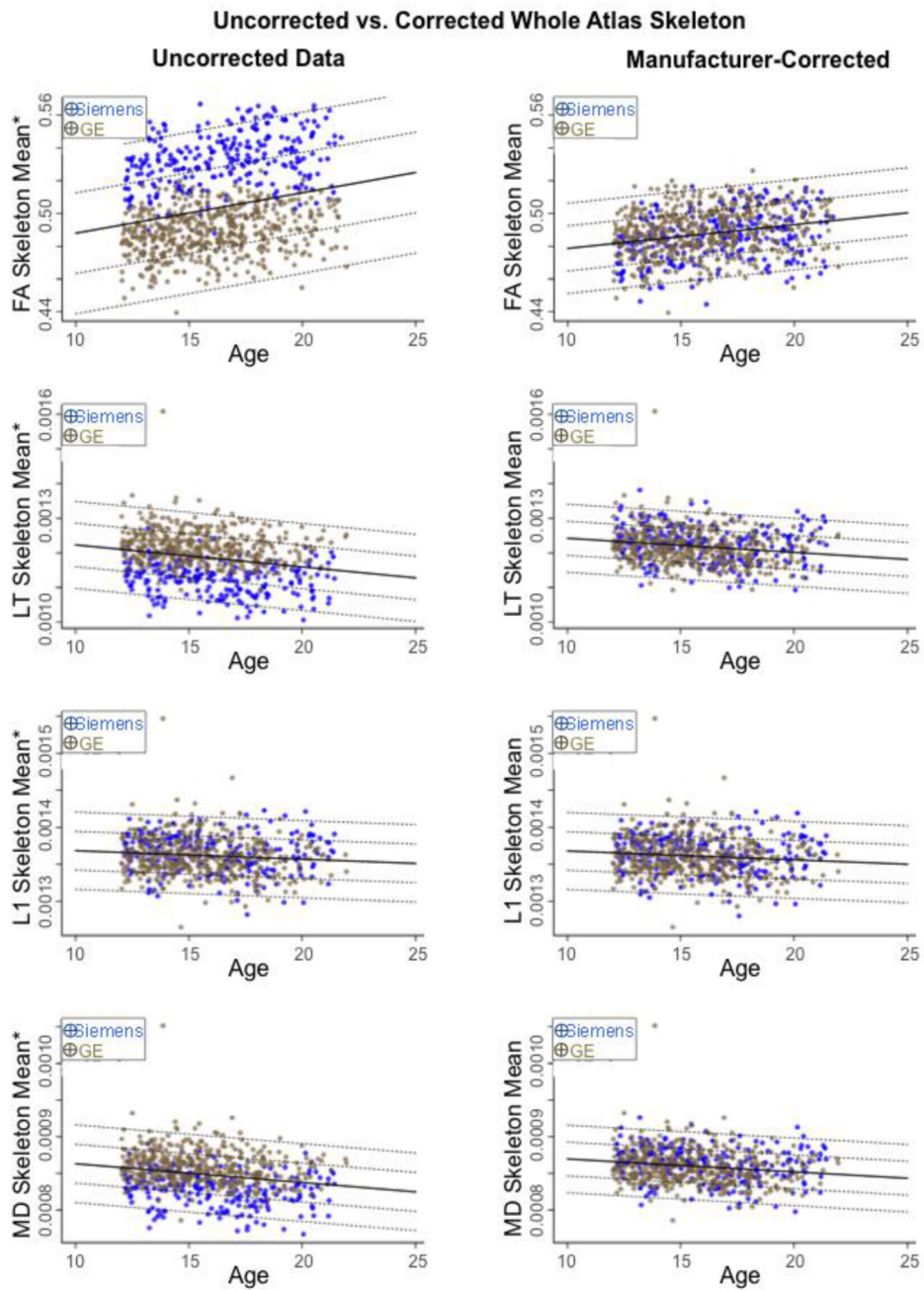
Figure 4.
Uncorrected whole-atlas FA skeleton mean for FA, MD, L1, and LT for Siemens (blue) and GE (gold) before (left) and after (right) application of the human phantom correction.

* Values are not corrected for sex, sex, race, and svol.
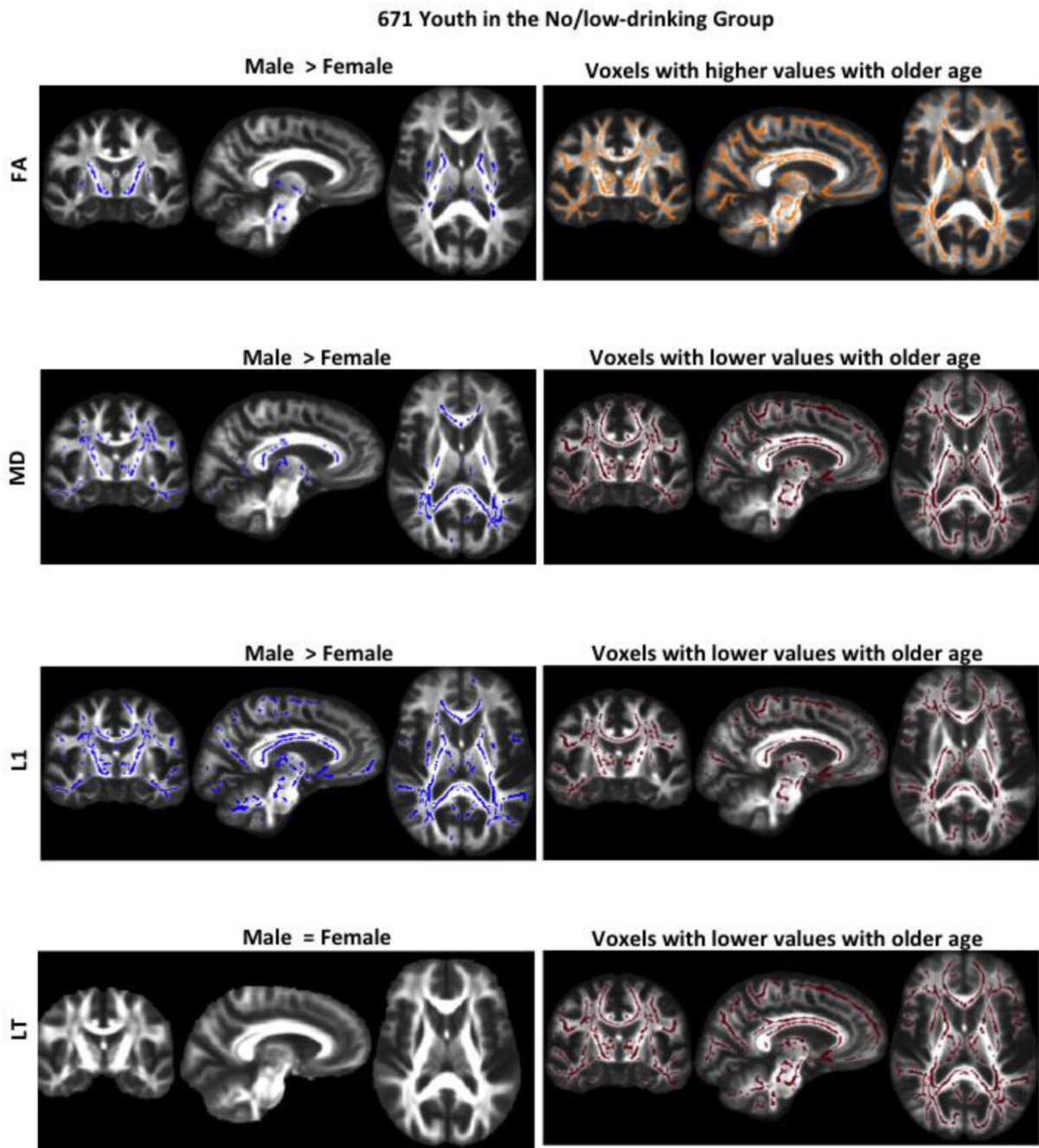
Figure 5.
Results of permutation testing demonstrating voxels in which boys had higher FA, MD, and L1 than girls (top) and voxels in which FA was higher and MD lower with older age (bottom).
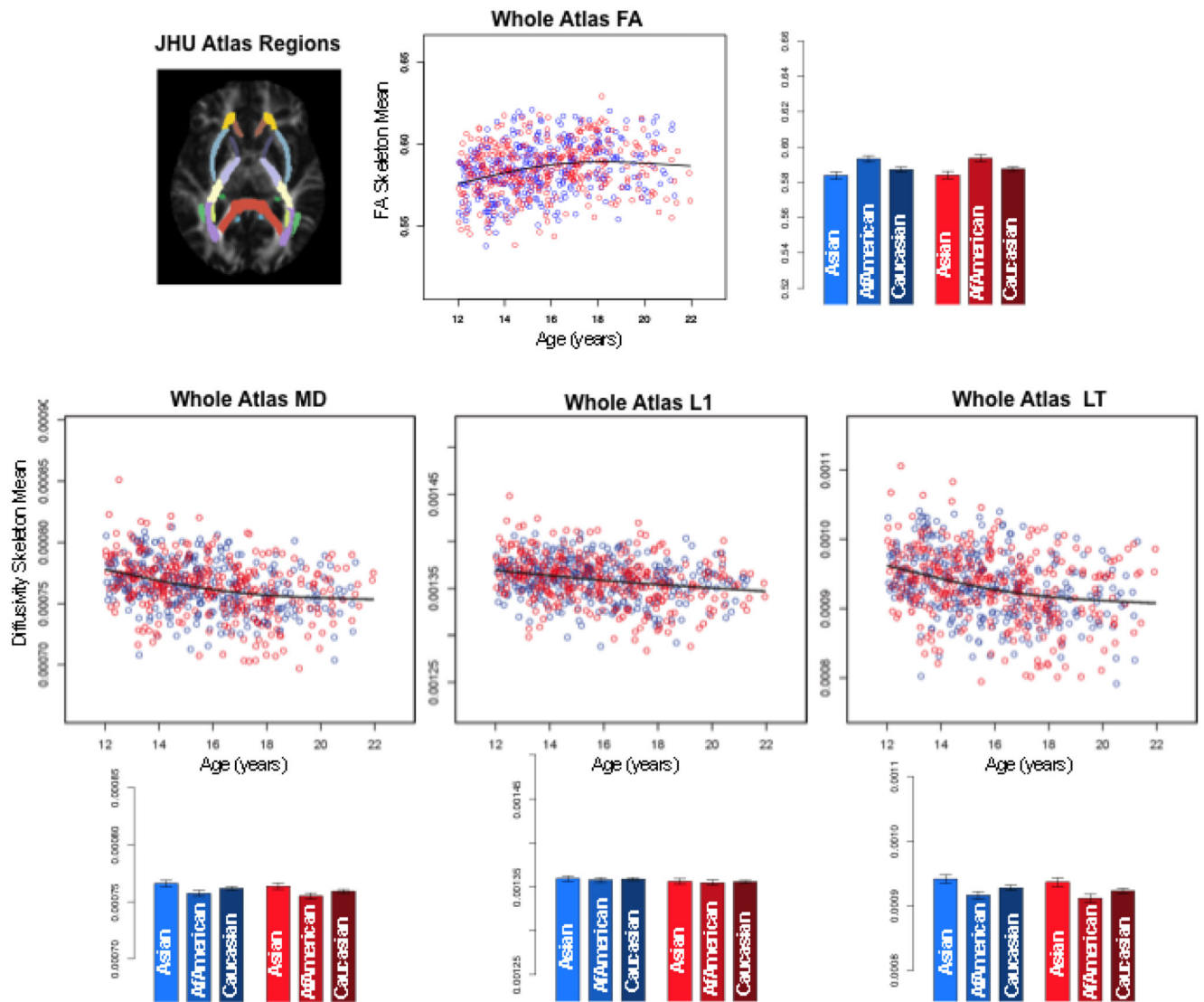
Figure 6.
Left: FA image with whole-atlas color-coded parcellations. Middle: Scatterplots showing the subject specific means of the whole-atlas skeleton FA, MD, L1, and LT, each corrected for sex, race, and svol differences in addition to type of manufacturer based on our correction ratio. Right: Bar graphs of predicted FA, MD, L1, and LT values for a 16-year old by sex and ethnicity (boys in blue; girls in red).
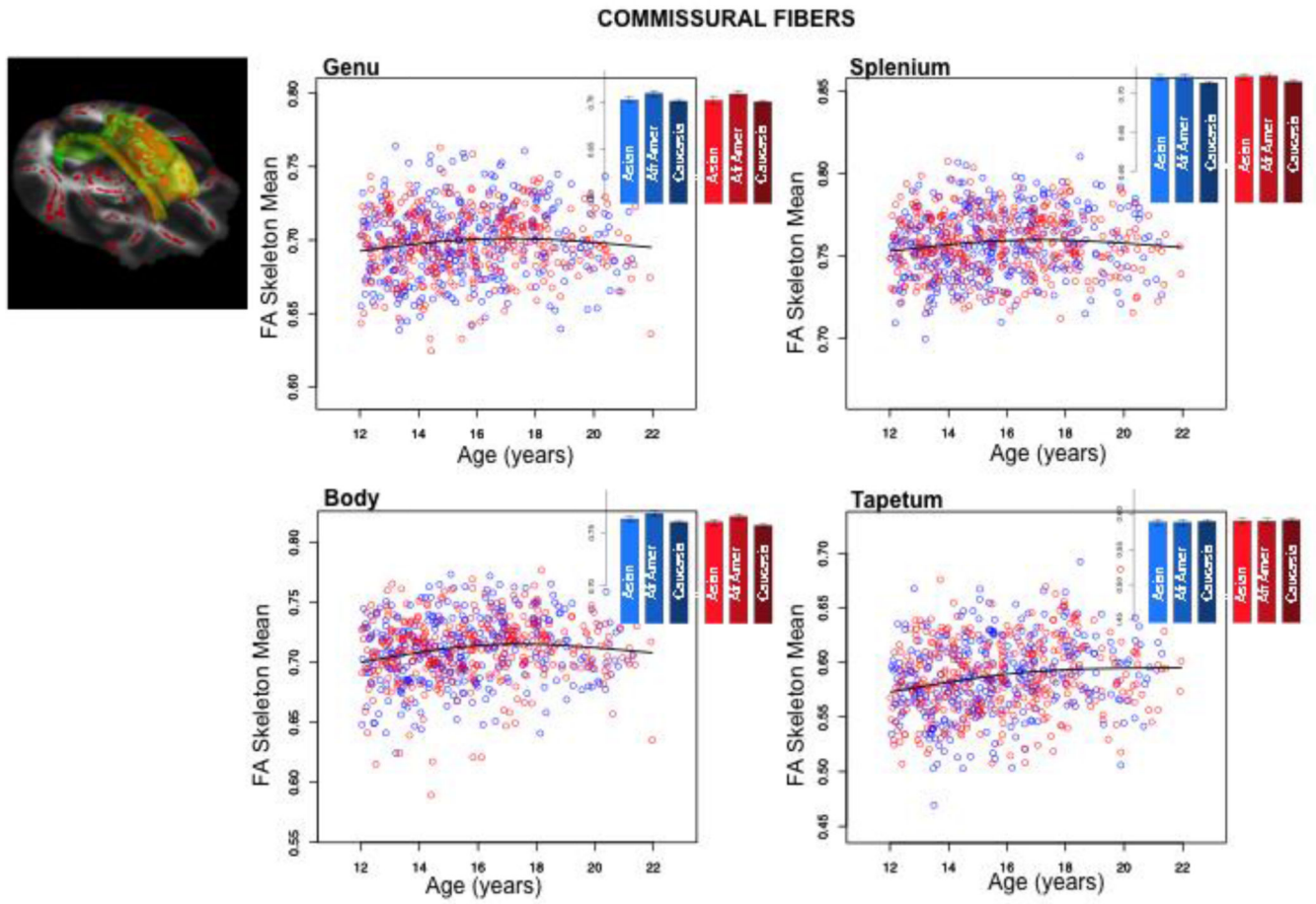
Figure 7.

FA image displaying commissural fibers. Scatterplots showing commissural fibers skeleton FA mean as a function of age. Bar graphs of predicted FA values for a 16-year old by sex and ethnicity (boys in blue; girls in red).
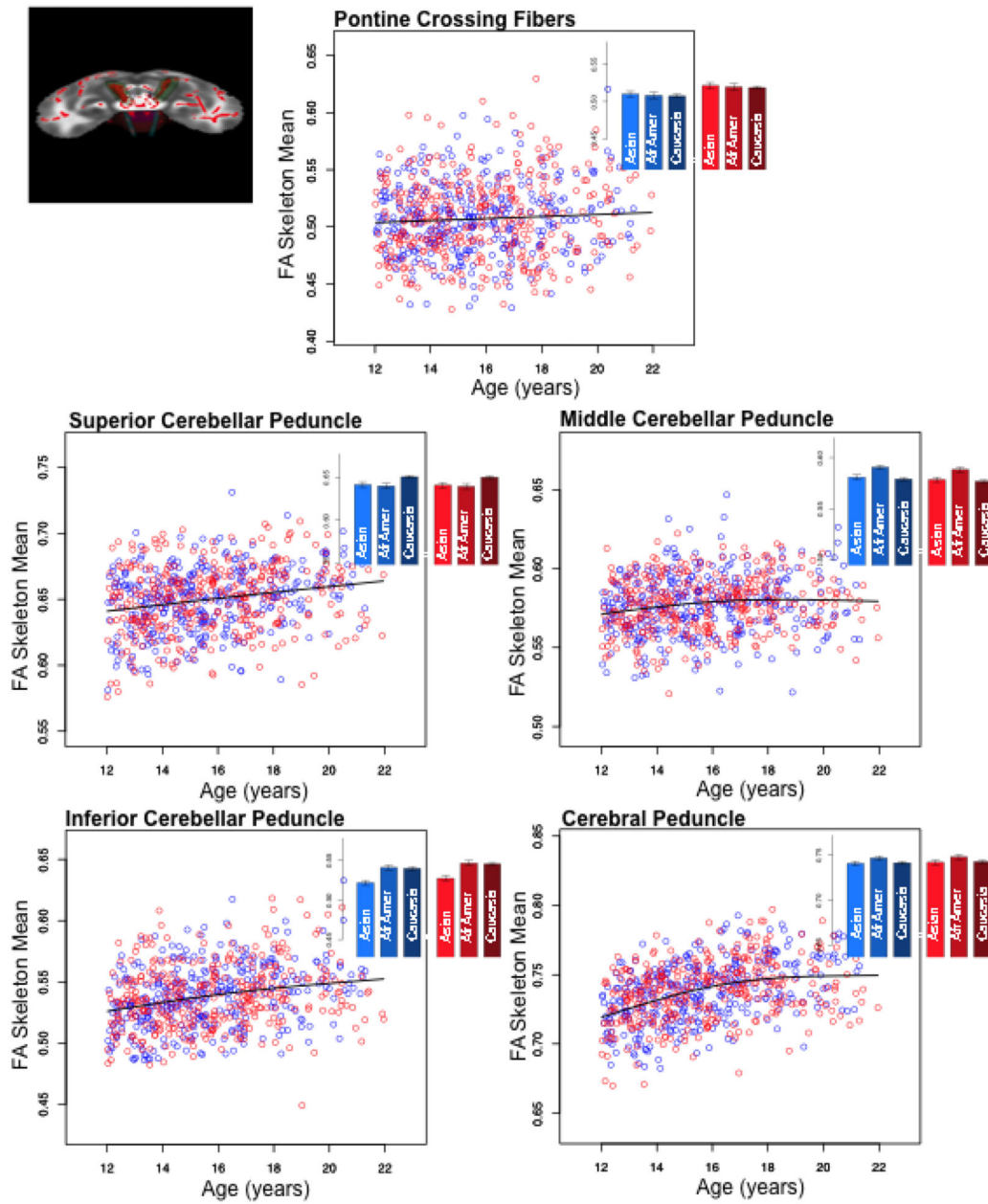
Figure 8.
FA image displaying brainstem projection fibers. Scatterplots showing brainstem projection fibers skeleton FA mean as a function of age. Bar graphs of predicted FA values for a 16-year old by sex and ethnicity (boys in blue; girls in red).

PROJECTION FIBERS: Corticospinal Tracts (PART 1)
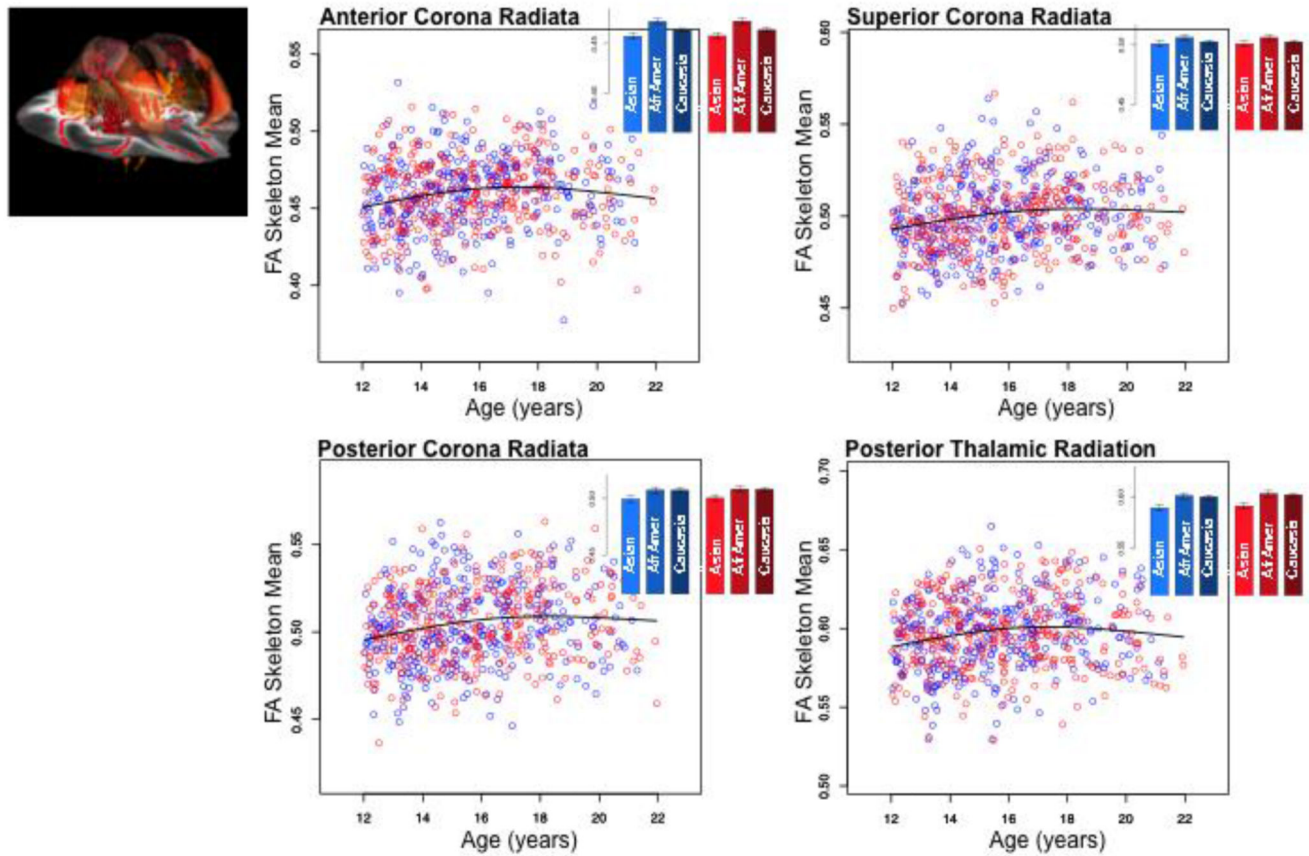
Figure 9.
FA image displaying corticospinal projection fibers (part 1). Scatterplots showing corticospinal projection fibers skeleton FA mean as a function of age. Bar graphs of predicted FA values for a 16-year old by sex and ethnicity (boys in blue; girls in red).

PROJECTION FIBERS: Corticospinal Tracts (PART 2)
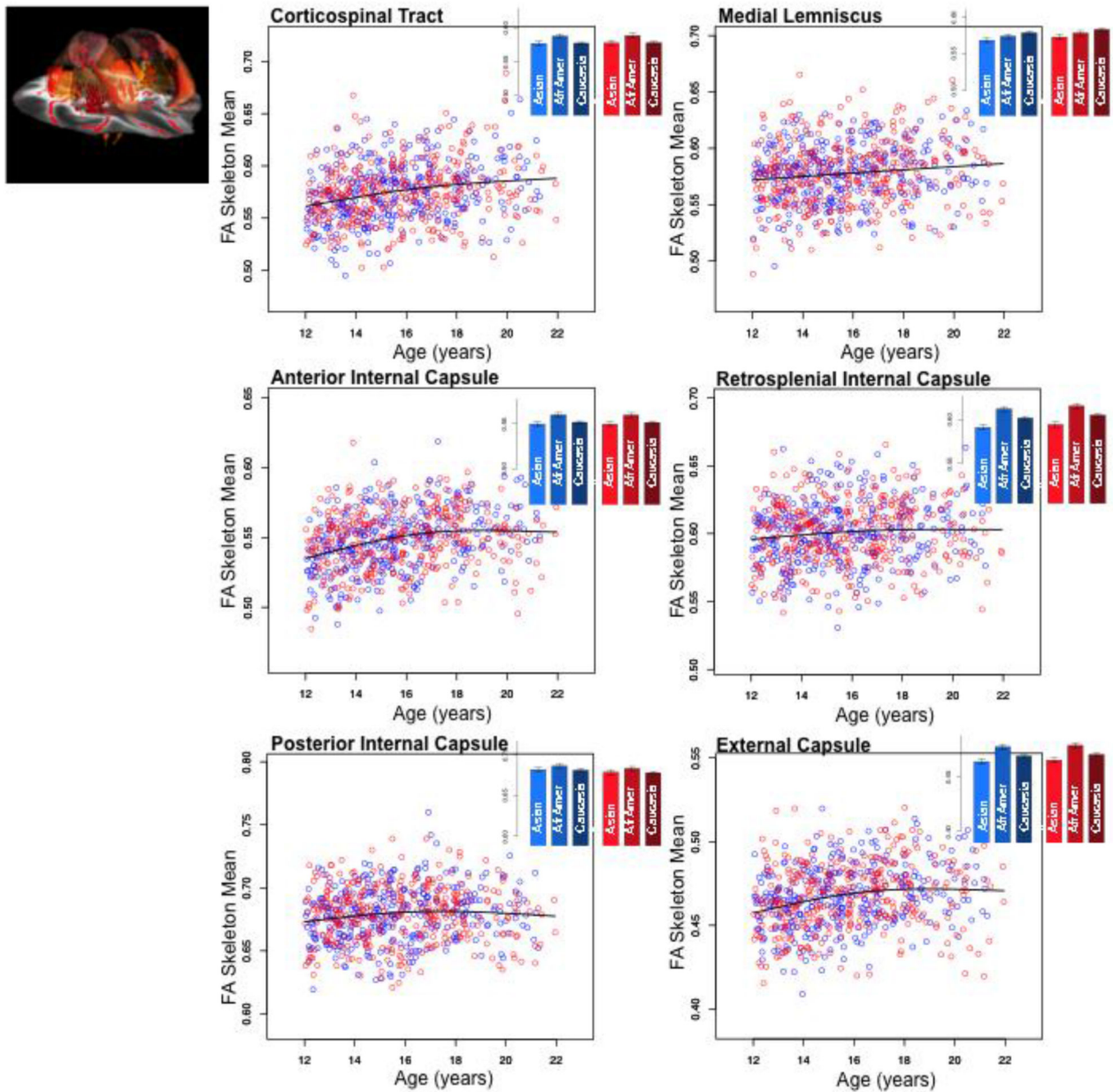
Figure 10.
FA image displaying corticospinal projection fibers (part 2). Scatterplots showing corticospinal projection fibers skeleton FA mean as a function of age. Bar graphs of predicted FA values for a 16-year old by sex and ethnicity (boys in blue; girls in red).
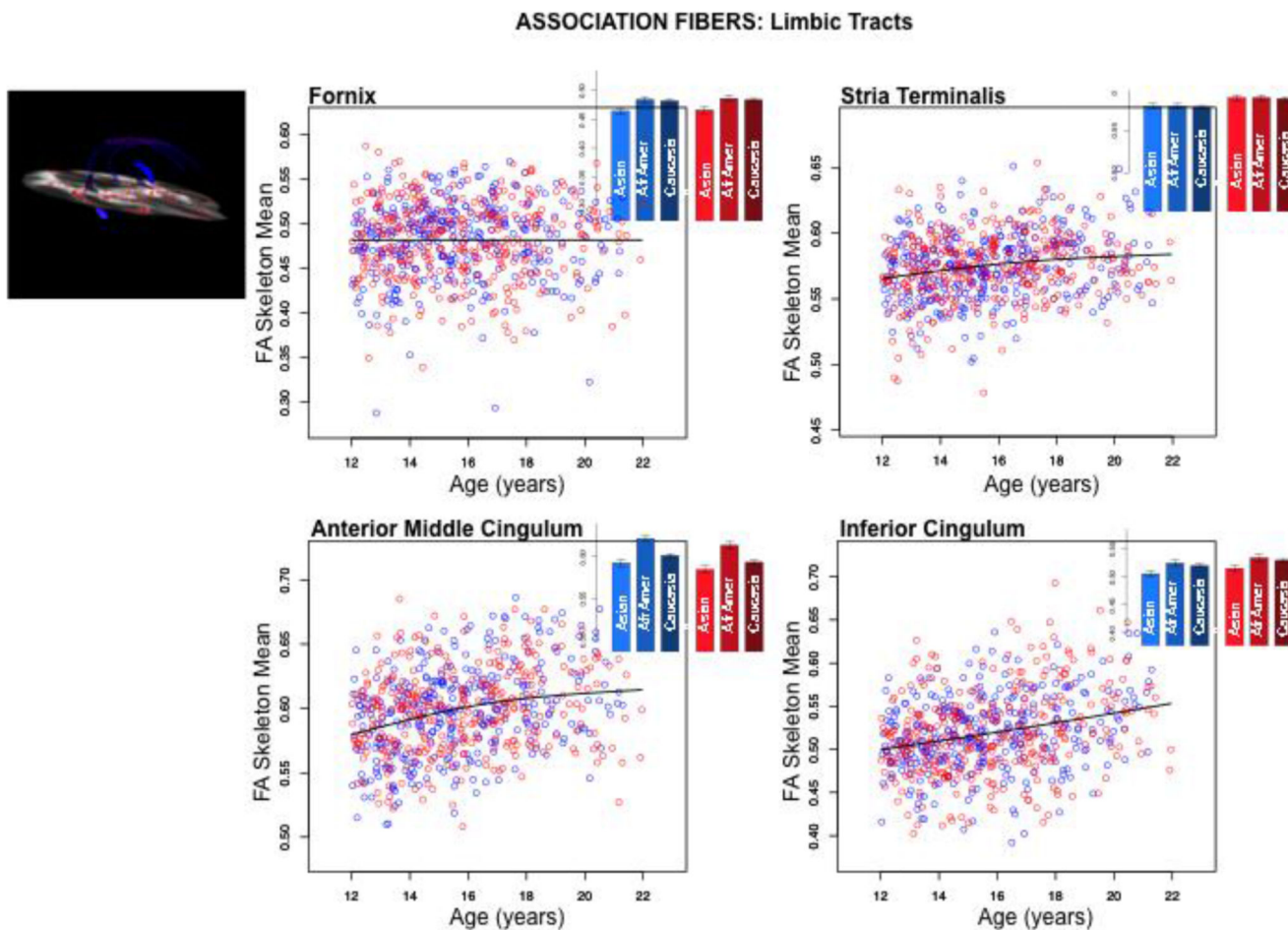
Figure 11.
FA image displaying limbic association fibers. Scatterplots showing limbic association fibers skeleton FA mean as a function of age. Bar graphs of predicted FA values for a 16-year old by sex and ethnicity (boys in blue; girls in red).
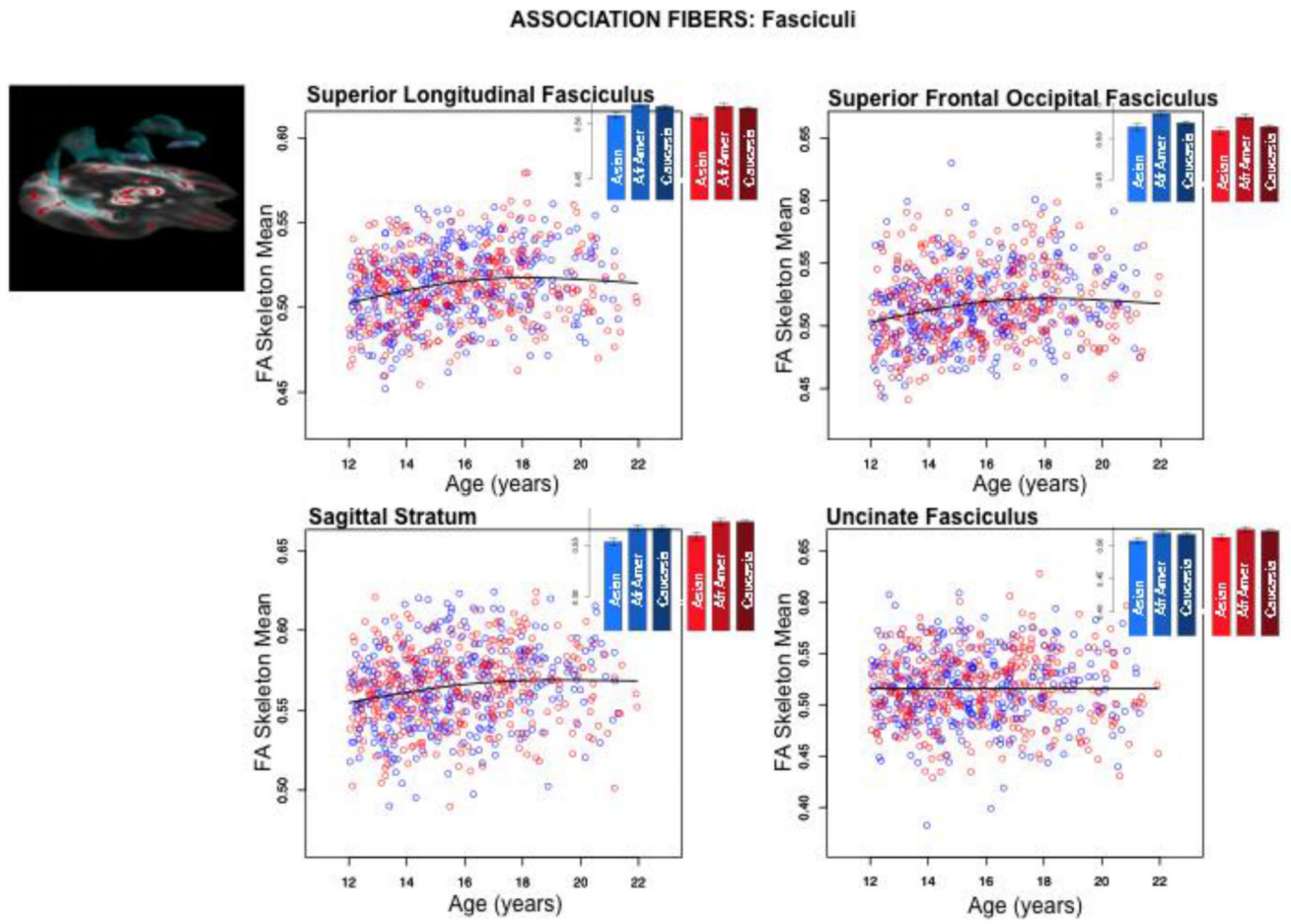
Figure 12.
FA image displaying association fasciculi. Scatterplots showing association fasciculi skeleton FA mean as a function of age. Bar graphs of predicted FA values for a 16-year old by sex and ethnicity (boys in blue; girls in red).

Table 1

NCANDA DTI group demographics (N=803)

		No/Low Drinker (N=671)		Exceeds-Criteria Youth (132)	
		Male	**Female**	**Male**	**Female**
	N	333	338	63	69
Age (years)	**mean**	15.6	15.8	18.5	18.6
	SD	2.3	2.4	2.0	1.9
	N	333	338	63	69
Education (years)	**mean**	8.9	9.2	11.7	11.9
	SD	2.3	2.5	1.9	1.9
	N	332	336	63	68
Pubertal Development Scale	**mean**	2.9	3.4	3.5	3.8
	median	3.0	3.6	3.6	4.0
	SD	0.7	0.6	0.5	0.2
	N	328	335	62	67
Socioeconomic Status	**mean**	17.1	16.6	17.2	17.2
	SD	2.4	2.5	2.1	2.3
	N	315	316	53	52
Handedness	**L/R/A**	31/254/48	19/285/34	2/52/9	6/56/7
	N	333	338	63	69
Family History of Alcoholism					
	negative/positive	308/25	308/30	49/14	60/9
Body Mass Index Percentile	**mean**	56.6	60.5	58.8	51.4
	SD	29.9	27.7	26.6	24.6
	N	329	335	61	69
Self-declared Ethnicity	**N**	333	338	63	69
Caucasian		244	228	51	54
African-American		32	52	3	8
Asian		27	25	6	4
Pacific Islander		1	3	0	0
American Indian		3	0	0	0
Mixed		26	30	3	3

Table 2

Age modeled with and without controlling for sex, ethnicity, and supratentorial volume (svol)

Skeleton Regions	No Covariates[1]		3 Covariates[2]				4 covariates[3]
	Age % Devian. explained	Age at max FA Confidence Interval	Age % Devian. explained	Age at max FA Confidence Interval	Age better fit	spline p-value	Age at max FA Confidence Interval
GLOBAL MORI SKELETON	6.46	[17.82,17.91]	10.60	[18.15,18.25]	spline	0.0003	[18.95,19.05]
COMMISSURAL FIBERS							
Genu	**1.60**	[16.78,16.86]	3.89	[17.02,17.11]	spline	0.0060	[17.65,17.74]
Body	**2.74**	[17.27,17.35]	**5.17**	[17.41,17.47]	spline	0.0036	[18.53,18.62]
Splenium	**1.35**	[16.86,16.94]	3.89	[17.11,17.17]	spline	0.0082	[21.91,21.95]
Tapetum	**3.74**	[21.91,21.95]	**4.45**	[21.91,21.95]	spline	0.0393	[19.61,19.66]
PROJECTION FIBERS							
Brainstem Tracts							
Pontine Crossing Fibers	0.75	[21.91,21.95]	3.19	[21.91,21.95]	linear	0.1653	[21.91,21.95]
Inferior Cerebellar Peduncle	**6.56**	[21.91,21.95]	**12.50**	[21.91,21.95]	spline	0.0719	[21.91,21.95]
Middle Cerebellar Peduncle	**2.30**	[17.87,17.95]	**7.07**	[18.51,18.56]	spline	0.0232	[21.91,21.95]
Superior Cerebellar Peduncle	**5.03**	[21.91,21.95]	**16.60**	[21.91,21.95]	spline	0.1087	[21.91,21.95]
Cerebral Peduncle	**15.70**	[20.41,20.46]	**19.01**	[21.91,21.95]	spline	0.0003	[21.91,21.95]
Corticospinal Tracts							
Corticospinal Tract	**6.20**	[21.91,21.95]	**8.36**	[21.91,21.95]	spline	0.0485	[21.91,21.95]
Medial Lemniscus	**2.11**	[21.91,21.95]	**7.96**	[21.91,21.95]	spline	0.0383	[21.15,21.21]
Anterior Internal Capsule	**7.78**	[18.41,18.46]	**17.00**	[19.01,19.06]	spline	0.0008	[19.41,19.45]
Poserior Internal Capsule	**1.40**	[17.21,17.27]	2.70	[17.41,17.47]	spline	0.0131	[21.91,21.95]
Retrosplenial Internal Capsule	**1.20**	[17.61,17.67]	7.02	[19.75,19.84]	spline	0.0609	[19.41,19.46]
Anterior Corona Radiata	**2.76**	[17.05,17.15]	**6.06**	[17.23,17.32]	spline	0.0015	[18.21,18.26]
Superior Corona Radiata	**3.12**	[18.01,18.07]	**3.87**	[18.27,18.35]	spline	0.0104	[19.81,19.86]
Poserior Corona Radiata	**3.73**	[18.05,18.14]	**6.59**	[18.17,18.25]	spline	0.0056	[18.32,18.41]
Posterior Thalamic Radiation	**2.69**	[17.31,17.37]	**5.50**	[17.32,17.41]	spline	0.0035	[17.35,17.44]
External Capsule	**5.21**	[18.21,18.26]	**11.80**	[18.84,18.93]	spline	0.0036	[21.91,21.95]
ASSOCIATION FIBERS							
Limbic Tracts							
Fornix	0.00	[21.91,21.95]	2.89	[21.91,21.95]	linear	0.3886	[21.91,21.95]
Stria Terminalis	**4.13**	[21.91,21.95]	**10.50**	[21.91,21.95]	spline	0.0698	[21.91,21.95]
Anterior Middle Cingulum	**7.15**	[21.91,21.95]	**14.40**	[21.91,21.95]	spline	0.0256	[21.91,21.95]
Inferior Cingulum	**7.85**	[21.91,21.95]	**13.80**	[21.91,21.95]	spline	0.1252	[21.91,21.95]
Fasciculi							
Superior Longitudinal Fasciculus	**4.67**	[17.91,17.97]	**8.05**	[18.11,18.15]	spline	0.0019	[18.51,18.56]

Skeleton Regions	No Covariates[1]		Age % Devian. explained	3 Covariates[2]			4 covariates[3]
	Age % Devian. explained	Age at max FA Confidence Interval		Age at max FA Confidence Interval	Age better fit	spline p-value	Age at max FA Confidence Interval
Superior Frontal-Occipital Fasciculus	**3.63**	[17.53,17.62]	**9.41**	[18.04,18.13]	spline	0.0035	[18.02,18.11]
Sagittal Stratum	**3.35**	[19.15,19.25]	**7.53**	[19.24,19.32]	spline	0.0241	[20.01,20.06]
Uncinate Fasciculus	0.54	[21.91,21.95]	4.65	[21.91,21.95]	linear	0.7327	[21.91,21.95]

Bold numbers indicate statistical significance based on adjustment for 28 comparisons, p .002; **99% confidence interval is listed for the age at maximum FA**

[1] No covariates entered into the model

[2] Maximum FA determined from model including sex, ethnicity, and svol as covariates applied to harmonized scores

[3] Maximum FA determined from model including sex, ethnicity, svol, and manufacturer as covariates applied to original scores

Table 3

Age modeled controlling for sex, ethnicity, and supratentorial volume (svol) with respect L1, LT, MD

Skeleton Regions	L1				LT				MD			
	Age % Devian. explained	Age at Min Confidence Interval	Age Better fit	Spline p-value	Age % Devian. explained	Age at Min Confidence Interval	Age Better fit	Spline p-value	Age % Devian. explained	Age at Min Confidence Interval	Age Better fit	Spline p-value
GLOBAL MORI SKELETON	22.90	[21.91,21.95]	spline	0.0745	**11.00**	[21.91,21.95]	spline	0.0156	**13.80**	[21.91,21.95]	spline	0.0104
COMMISSURAL FIBERS												
Genu	**7.19**	[21.91,21.95]	linear	0.0038	**3.85**	[21.91,21.95]	spline	0.0581	**5.43**	[21.91,21.95]	spline	1.000
Body	**9.60**	[21.91,21.95]	spline	1.0000	**6.79**	[21.91,21.95]	spline	0.0978	**6.63**	[21.91,21.95]	spline	0.1018
Splenium	13.90	[19.14,19.22]	spline	0.0564	**5.33**	[21.91,21.95]	spline	NA	**11.10**	[21.91,21.95]	spline	0.0972
Tapetum	**5.93**	[21.91,21.95]	linear	1.0000	**6.74**	[21.91,21.95]	spline	0.0841	**7.45**	[21.91,21.95]	spline	0.0756
PROJECTION FIBERS												
Brainstem Tracts												
Pontine Crossing Fibers	**5.26**	[18.55,18.64]	spline	0.0353	**3.44**	[21.91,21.95]	linear	0.0422	**4.42**	[21.91,21.95]	spline	0.0997
Inferior Cerebellar Peduncle	5.22	[12.02,12.10]	linear	0.9147	**9.28**	[21.91,21.95]	spline	0.1208	**5.53**	[21.91,21.95]	spline	1.0000
Middle Cerebellar Peduncle	3.33	[21.91,21.95]	linear	0.5563	**5.87**	[21.91,21.95]	spline	0.0601	5.47	[18.75,18.84]	spline	0.0389
Superior Cerebellar Peduncle	16.80	[21.91,21.95]	linear	0.2017	**11.00**	[21.91,21.95]	spline	1.000	**7.78**	[21.91,21.95]	spline	1.0000
Cerebral Peduncle	**13.30**	[21.91,21.95]	spline	0.1087	**18.10**	[21.91,21.95]	spline	1.000	**18.40**	[21.91,21.95]	spline	1.0000
Corticospinal Tracts												
Corticospinal Tract	2.21	[12.02,12.10]	linear	0.2677	2.78	[16.84,16.94]	spline	0.004	2.52	[16.43,16.52]	spline	0.0051
Medial Lemniscus	5.40	[21.91,21.95]	linear	0.1804	**5.21**	[21.91,21.95]	linear	0.0057	**3.09**	[21.91,21.95]	spline	0.0313
Anterior Internal Capsule	15.40	[21.91,21.95]	linear	0.7041	**11.40**	[21.91,21.95]	spline	0.0573	**10.10**	[21.91,21.95]	spline	0.1309
Posterior Internal Capsule	**13.20**	[21.91,21.95]	spline	0.1067	**6.12**	[21.91,21.95]	spline	0.0977	**14.70**	[21.91,21.95]	spline	0.0255
Retrosplenial Internal Capsule	**14.00**	[21.91,21.95]	spline	0.0506	**5.73**	[21.91,21.95]	spline	0.0537	**6.97**	[21.91,21.95]	spline	0.094

Skeleton Regions	L1				LT				MD			
	Age % Devian. explained	Age at Min Confidence Interval	Age Better fit	Spline p-value	Age % Devian. explained	Age at Min Confidence Interval	Age Better fit	Spline p-value	Age % Devian. explained	Age at Min Confidence Interval	Age Better fit	Spline p-value
Anterior Corona Radiata	**13.00**	[20.81,20.85]	spline	0.0188	**7.76**	[17.83,17.92]	spline	0.0001	**10.80**	[18.11,18.17]	spline	0.000
Superior Corona Radiata	**10.20**	[21.91,21.95]	spline	1.0000	**8.53**	[21.91,21.95]	spline	0.0094	**12.60**	[21.91,21.95]	spline	0.0173
Posterior Corona Radiata	**14.10**	[18.31,18.36]	spline	0.0085	**7.85**	[18.41,18.46]	spline	0.0007	**10.40**	[18.35,18.45]	spline	0.0002
Posterior Thalamic Radiation	**14.10**	[21.91,21.95]	spline	0.0751	**7.69**	[21.91,21.95]	spline	0.0541	**11.20**	[21.91,21.95]	spline	0.047
External Capsule	12.60	[21.91,21.95]	linear	0.8123	**8.01**	[18.32,18.41]	spline	0.0014	**6.82**	[18.11,18.17]	spline	0.0027
ASSOCIATION FIBERS												
Limbic Tracts												
Fornix	2.68	[12.02,12.10]	spline	0.0539	1.05	[12.02,12.10]	linear	0.2043	1.28	[12.02,12.10]	linear	0.2243
Stria Terminalis	20.40	[21.91,21.95]	linear	0.2465	**8.22**	[21.91,21.95]	spline	0.0993	**9.53**	[21.91,21.95]	spline	0.0997
Anterior Middle Cingulum	4.33	[12.02,12.10]	linear	0.1175	**13.40**	[21.91,21.95]	spline	0.112	**6.11**	[21.91,21.95]	spline	0.0586
Inferior Cingulum	**22.20**	[21.91,21.95]	spline	0.0964	**13.90**	[21.91,21.95]	spline	1.000	**18.00**	[21.91,21.95]	spline	1.0000
Fasciculi												
Superior Longitudinal Fasciculus	11.10	[21.91,21.95]	linear	0.1836	**8.35**	[19.11,19.16]	spline	0.0049	**8.81**	[19.11,19.16]	spline	0.008
Superior Frontal-Occipital Fasciculus	**12.10**	[21.91,21.95]	spline	0.0548	**7.65**	[21.91,21.95]	spline	0.0586	**9.75**	[21.91,21.95]	spline	1.000
Sagittal Stratum	14.20	[21.91,21.95]	linear	0.2331	**9.78**	[21.91,21.95]	spline	0.066	**11.70**	[21.91,21.95]	spline	0.0334
Uncinate Fasciculus	4.34	[21.91,21.95]	linear	0.4908	3.05	[21.91,21.95]	linear	0.2816	1.52	[21.91,21.95]	linear	0.2946

Bold=significance based on adjustment for 28 comparisons, p .002; 99% confidence interval for age at maximum FA